EXPERIMENTAL INVESTIGATION OF TWO BLUNT TRAILING EDGE SUPERSONIC COMPRESSOR ROTORS OF DIFFERENT BLADE THICKNESSES AND WITH CIRCULAR ARC CAMBER LINE

C. T. Carman and J. R. Myers
ARO, Inc.
and
A. J. Wennerstrom and John W. Steurer
Aerospace Research Laboratories

September 1968

ENGINEERING SUPPORT FACILITY
ARNOLD ENGINEERING DEVELOPMENT CENTER
AIR FORCE SYSTEMS COMMAND
ARNOLD AIR FORCE STATION, TENNESSEE

NOTICES

When U. S. Government drawings specifications, or other data are used for any purpose other than a definitely related Government procurement operation, the Government thereby incurs no responsibility nor any obligation whatsoever, and the fact that the Government may have formulated, furnished, or in any way supplied the said drawings, specifications, or other data, is not to be regarded by implication or otherwise, or in any manner licensing the holder or any other person or corporation, or conveying any rights or permission to manufacture, use, or sell any patented invention that may in any way be related thereto.

Qualified users may obtain copies of this report from the Defense Documentation Center.

References to named commercial products in this report are not to be considered in any sense as an endorsement of the product by the United States Air Force or the Government.

ERRATA

AEDC-TR-68-197, September 1968

EXPERIMENTAL INVESTIGATION OF TWO BLUNT TRAILING EDGE SUPERSONIC COMPRESSOR ROTORS OF DIFFERENT BLADE THICKNESSES AND WITH CIRCULAR ARC CAMBER LINE

C. T. Carman and J. R. Myers, ARO, Inc.
A. J. Wennerstrom and John W. Steurer, Aerospace Research Laboratories

Arnold Engineering Development Center
Air Force Systems Command
Arnold Air Force Station, Tennessee

Please substitute these Figs. IV-1a and b for those on pages 30 and 31 in subject report.

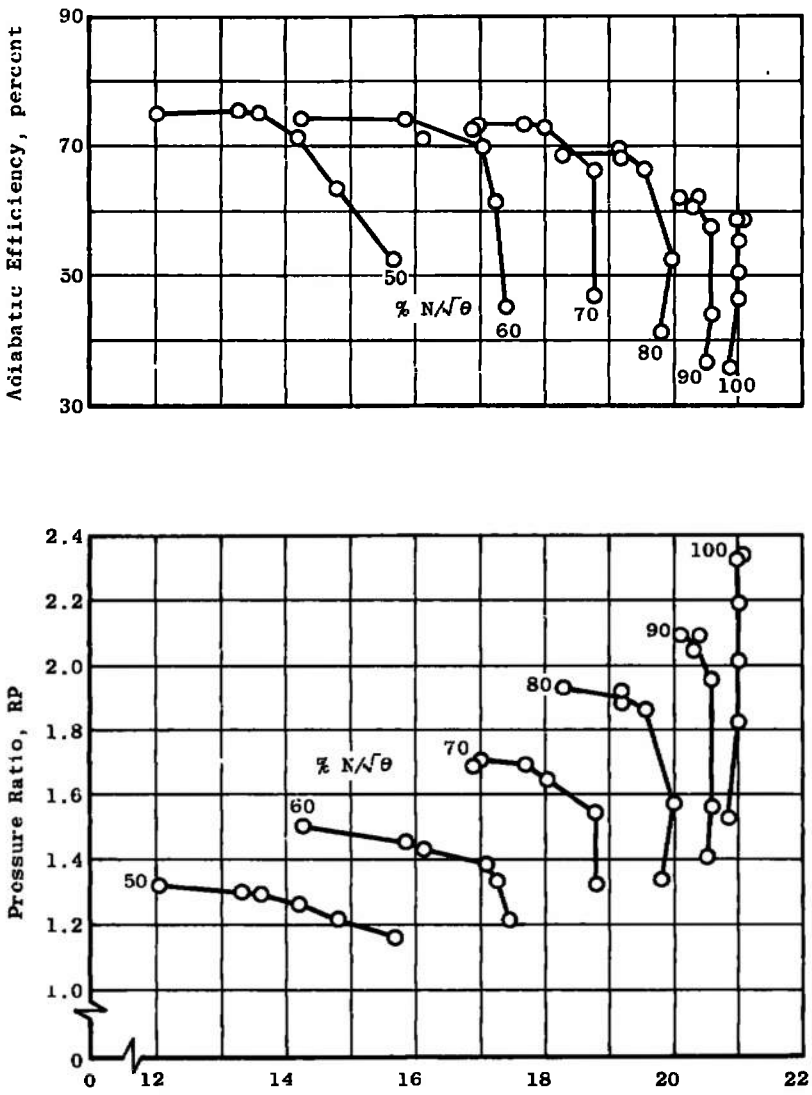

a. Compressor Performance Characteristics Based on Equivalent Weight Flow

Fig. IV-1 Configuration 1

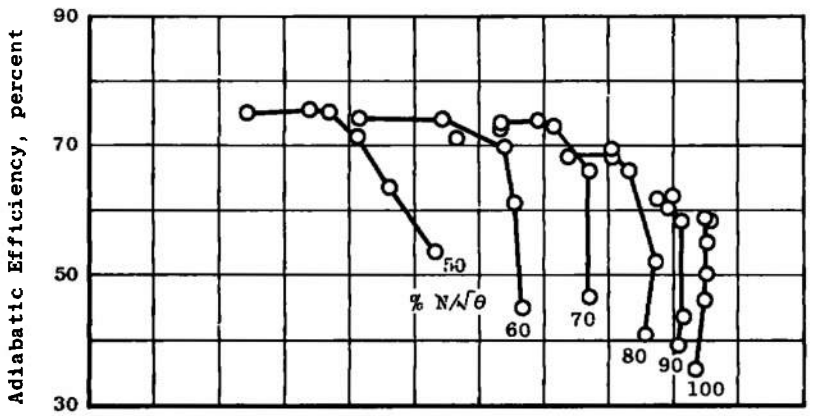

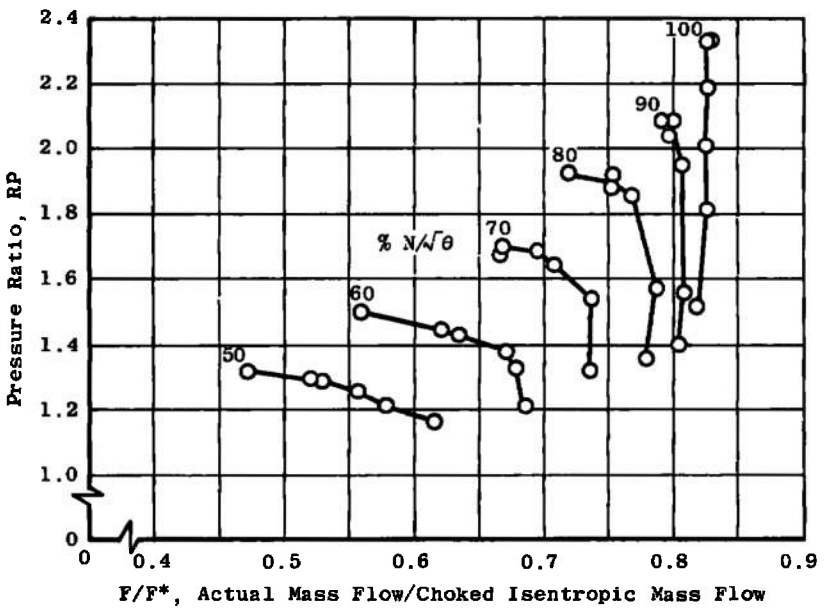

b. Compressor Performance Characteristics Based on Weight Flow Ratio
Fig. IV-1 Continued

EXPERIMENTAL INVESTIGATION OF TWO BLUNT TRAILING EDGE SUPERSONIC COMPRESSOR ROTORS OF DIFFERENT BLADE THICKNESSES AND WITH CIRCULAR ARC CAMBER LINE

C. T. Carman and J. R. Myers
ARO, Inc.

and

A. J. Wennerstrom and John W. Steurer
Aerospace Research Laboratories

AF - AEDC
Arnold AFS Tenn

FOREWORD

This report was prepared by Messrs. C. T. Carman and J. R. Myers of ARO, Inc. (a subsidiary of Sverdrup & Parcel and Associates, Inc.), contract operator of the Arnold Engineering Development Center (AEDC), Air Force Systems Command (AFSC), Arnold Air Force Station, Tennessee, and Dr. Arthur J. Wennerstrom and 1st Lt John W. Steurer of the Fluid Dynamics Facilities Research Laboratory of the Aerospace Research Laboratories, OAR, Wright-Patterson Air Force Base, Ohio.

Aerodynamic design and analysis of the compressor rotors were conducted at the Aerospace Research Laboratories. Mechanical design and all experimental work were conducted at the Arnold Engineering Development Center. The complete program was sponsored by the Aerospace Research Laboratories under Program Element 6144501F, Project 7065, "Aerospace Simulation Techniques Research," under the direction of Mr. Elmer G. Johnson. The work was performed between August 1965 and January 1967. The report was submitted for publication on August 12, 1968.

This technical report has been reviewed and is approved.

Hans K. Doetsch
Technical Advisor
Directorate of Plans
and Technology

Edward R. Feicht
Colonel, USAF
Director of Plans
and Technology

ABSTRACT

Two configurations of blunt-trailing-edge supersonic compressor blades were tested with air in the AEDC compressor rig. The performance of these blades was investigated over the speed range from 50 to 100 percent of design speed. The performance of the two blade configurations is compared, and the effect of the modifications between the two configurations is evaluated.

CONTENTS

APPENDIXES

I. ILLUSTRATIONS

Figure

NOMENCLATURE

A	Area, $in.^2$
C	Absolute velocity, ft/sec
C_f	Flow coefficient
C_p	Specific heat at constant pressure
d	Axial distance from blade leading edge, in.
F	Weight flow, lb/sec
G	Specific weight flow, $lb/sec\text{-}in.^2$
g	Local acceleration of gravity, 32.14 ft/sec^2
H	Enthalpy
IW	Inner wall of compressor annulus
J	Mechanical equivalent of heat, 778.3 ft-lb/Btu
M	Mach number
N	Rotational speed, rpm
OW	Outer wall of compressor annulus
P	Total pressure, psia
p	Static pressure, psia
R	Gas constant for air, 53.34 ft-lb/lb°R
Re	Reynolds number
RF	Thermocouple impact-recovery factor

RP	Pressure ratio
r	Radius, in.
T	Total temperature, °R
t	Static temperature, °R
U	Circumferential blade velocity, ft/sec
W	Relative velocity, ft/sec
α	Absolute flow angle relative to axis of rotation, deg
β	Relative flow angle
γ	Ratio of specific heats
δ	Ratio of inlet total pressure to the ARDC model sea-level atmosphere (14.7 psia)
$\sqrt{\theta}$	Ratio of inlet absolute total temperature to absolute total temperature of ARDC model sea-level atmosphere (519.3°R)

SUBSCRIPTS

0, 1, 2, 3	Compressor instrumentation stations
a	Adiabatic
av	Average
calc	Calculated
deg	Degrees
i	Indicated
isen	Isentropic
w	Relative

SECTION I
INTRODUCTION

This is the first of a series of reports which present detailed experimental data from the supersonic compressor research program of the Aerospace Research Laboratories. The experimental portion of this program is being conducted at the Arnold Engineering Development Center. To date, the program has only considered rotors of relatively high solidity which employ blades having blunt trailing edges; i.e., the maximum blade thickness is at 100 percent chord. This design concept was first proposed in Ref. 1. The blading is designed so that the flow passages have relatively constant area and, as a result of camber, the trailing edges remain blunt. The geometry is arranged with a suitable passage length-to-width ratio in such a way that a pseudo-shock diffusion is encouraged between blades. The flow at the trailing edges is allowed to undergo a sudden-area-increase diffusion process which is reasonably efficient if the trailing edge Mach number is not close to unity. A complete discussion of the design philosophy is given in Ref. 2.

Limited testing of the 5-in. rotor described in Ref. 1 provided some encouraging results. Therefore, the initial tests of the current 22-in.-diam rotor were undertaken to evaluate the proposed design concepts.

The overall performance of the first configuration tested was discussed and compared with a theoretical analysis in Ref. 3. In general, the performance was poor. The maximum pressure ratio attained was 2.34 at an adiabatic efficiency of only 59 percent. However, the theoretical analysis suggested that this performance could be improved by incorporating the following modifications: (1) a reduction in the blade trailing-edge thickness, (2) a redistribution of the blade camber, and (3) annulus contouring.

The purpose of this series of reports is twofold: First, to present the complete set of data for the configurations tested; secondly, to present the data in a manner which allows the merits of the above modifications to be evaluated. This report specifically deals with the effects of reducing the blade trailing-edge thickness or, preferably, the blade thickness-to-spacing ratio (t/s). Subsequent reports will deal with the other suggested modifications.

Data from two rotors are presented and compared in this report. Both rotors employ circular arc blade surfaces. The rotors differ only in the blade thickness at the trailing edge and, as a consequence, in the amount of divergence in passage area which occurs through the blade row. All other characteristics are identical. The increased passage divergence was achieved by generating new circular arc surfaces around the camber line of the first rotor in a manner which reduced the blade thickness.

SECTION II
APPARATUS

2.1 COMPRESSOR DESIGN

The rotor configurations described in this report were designed to provide a direct continuation of the work reported in Ref. 1; however, the configurations were of larger scale than those discussed in Ref. 1 so that more detailed and accurate measurements could be taken. Therefore, no new thinking was applied to the basic aerodynamic design of the rotors reported herein. A mid-radius inlet blade angle of 60 deg (from axial) and a mid-radius exit blade angle of 30 deg were employed, resulting in a camber of 30 deg, as before. Because the design philosophy intended to employ a pseudo-shock diffusion process, a solidity of 3.0 was chosen to provide a relatively high passage length-to-width ratio. It was hoped to achieve a total pressure ratio of approximately 3.0 at a corrected tip speed of 1600 ft/sec. The mean-radius relative inlet Mach number at design speed and zero incidence would be 1.7.

The hub/tip radius ratio for these tests was 0.9, and the rotor tip diameter was 22 in. The high hub/tip ratio was chosen in order to minimize inviscid three-dimensional flow effects. No hub or tip contouring was employed for the configurations presented in this report.

The blade surfaces at mid-radius were circular arcs extending from a small leading-edge radius to a point of maximum thickness at the trailing edge. The surfaces were symmetrical with respect to a circular arc camber line. Since the trailing edges end abruptly in sharp corners, the blades have the appearance of thin, curved wedges. The blade surfaces between hub and tip are formed by geometric spirals passing through the circular arcs at mid-radius. That is to say, a line passing through, and normal to, the compressor axis and which is moved through the outline of a mid-radius blade element will generate the blade surface from hub to tip. Thus, the pitch of the spiral surfaces is radially constant but axially variable. As a result, the blades are slightly thicker at the tip than at the root.

Because of the high solidity and relatively short chord length, 126 blades were required. Since blade attachment would have been excessively expensive, the blading was machined directly into the rim of the wheel.

The geometry of the first configuration at mid-radius is presented in Fig. 1a. Minimum flow area between blades occurs on a surface extending from the base of the leading-edge radius of one blade to the nearest point on the suction surface of an adjacent blade. In the confined portion of the flow passage, this area increases approximately 10 percent from entrance to exit. A parameter which has proven useful for performance

calculations with blunt trailing-edge blades (see Ref. 3) is the ratio of trailing-edge thickness to blade spacing, measured circumferentially. The thickness-to-spacing ratio for this first rotor was 0.395.

The geometry of the second configuration at mid-radius is presented in Fig. 1b. This differs from the first in that the thickness-to-spacing ratio has been reduced to 0.272, resulting in a larger increase in flow area between the passage entrance and exit. For this configuration the area increases approximately 27 percent. Theoretical calculations presented in Ref. 3 indicated that increased passage divergence should lead to an increase in performance, if boundary-layer blockage does not significantly increase. The particular value of 0.272 was chosen in order to enable comparison with data presented in Ref. 4 for a similar configuration.

2.2 COMPRESSOR RIG

Since complete details on the compressor rig are presented in Ref. 5, only a limited description is provided here. A cross section of the compressor is shown in Fig. 2. The incoming air is drawn from a large settling chamber containing a straightener and screens. The inner wall of the outer casing is completely cylindrical throughout the entire central section of the compressor, and the hub wall is also cylindrical downstream of the compressor. However, the base of the bulletnose which extends into the central section of the compressor is a 1.0-deg. cone to provide a slight flow acceleration all the way to the rotor leading-edge plane. The discharging flow enters a radial diffusing section which terminates in a circumferential throttle valve. The throttle valve has a series of equally spaced and sized discharge ports around the periphery to eliminate as much as possible any asymmetric conditions which might feed back to the compressor. No stator blade rows were used in conjunction with these experiments. The test rig is a closed-loop system, incorporating a heat exchanger and a venturi to measure mass flow in the return loop. Inlet total pressure and temperature were maintained at approximately standard atmospheric conditions, and all presented data are corrected to standard conditions.

2.3 INSTRUMENTATION

Aerodynamic pressures and/or temperatures are measured at the stations shown in Fig. 2. Axial and radial locations and details of the measuring stations in the compressor and venturi are shown in Fig. 3.

Total pressure and total temperature upstream of the rotor were measured with pairs of 5-element rakes placed 1.0 in. ahead of the rotor. These pressure probes were simple impact tubes since the flow direction is uniform and known. The temperature probes contain iron-constantan thermocouples in diffuser shrouds. The probe elements were centered at the centroids of circumferential bands of equal flow area. Total pressure and total temperature downstream of the rotor were each measured with a

pair of 5-element rakes placed 2.0 in. behind the rotor. These were similar to the upstream rakes, except that the pressure probes were of the directionally insensitive Kiel design. Radial traverses were made to measure total pressure and flow angle at locations 0.5 and 2.0 in. behind the rotor. Two- and three-hole prism-type yaw probes were used for measuring flow angle and flow angle plus total pressure. A row of static pressure taps of 0.025-in. diam were located in the outer casing beginning upstream, across, and downstream of the rotor. Additional static taps were placed at corresponding locations on the hub wall, up and downstream of the rotor.

The aerodynamic pressure data were measured with strain-gage transducers, and temperatures were measured with thermocouples. The outputs from these instruments are processed through an analog-to-digital converter and recording system. This system completed a scan of 100 channels in one minute.

SECTION III
PROCEDURE

The compressor rotors were tested between 50 and 100 percent design speed in increments of 10-percent speed. Design corrected tip speed was 1600 ft/sec. Performance data were measured at each speed from choked flow (wide open throttle) to audible surge. Three complete data scans were recorded at each test point, and the average values were used in the data reduction process. The yaw probes were traversed once during each test point.

SECTION IV
RESULTS AND DISCUSSION

4.1 GENERAL ROTOR PERFORMANCE

4.1.1 Rotor 1, Configuration 1

Complete experimental data for this configuration are presented as curves and tables in Appendix IV. Maximum design-speed pressure ratio was 2.34, at which point the adiabatic efficiency was 59 percent. Peak efficiency continuously increased as speed was reduced, reaching 76 percent at 50 percent speed. The relative inlet Mach number at design speed, and maximum pressure ratio, varied from 1.45 at the hub to about 1.56 at the tip.

Radial traverse data taken 0.5 in. downstream of the rotor show that flow separation occurred on the outer casing wall immediately downstream of the rotor at 90- and 100-percent speed. At 80-percent speed and below, this condition was not observed. From a comparison of data

over the speed range, it appears that relatively thick boundary layers develop in the blade passages as speed is increased and that much of this low-energy flow is centrifuged toward the tip as a secondary flow. This is probably a result of shock-induced suction surface separation leading to large cross flows in the separated region. The low-energy flow is unable to overcome the pressure gradient in the diffusion zone following the thick trailing edges at the higher speeds. This seriously distorts the rotor discharge profiles at intermediate speeds also.

The static pressure distributions along the annulus walls are tabulated in Appendix IV. At 100-percent speed, the compressor map showed that stall occurred before the bow shock was expelled from the flow passage between rotor blades, as evidenced by the vertical characteristic. This is confirmed by the casing static pressure distribution which shows a large passage entrance expansion before the first strong shock. At 90-percent and lower speeds, this entrance expansion is not evident at maximum back pressure. The annulus wall separation zone also produces a noticeable effect on the static pressure distributions. When separation occurs, the pressure gradient is sharply reduced.

The measured performance of this rotor is compared with some theoretical calculations in Ref. 3.

4.1.2 Rotor 1, Configuration 2

The experimental data for this configuration are also presented in Appendix IV. Maximum design-speed pressure ratio was 2.32, at which point the adiabatic efficiency was 57 percent. Peak efficiency continuously increased as speed was reduced, reaching 79 percent at 50 percent speed. The relative inlet Mach number distribution at design speed, and maximum pressure ratio, was the same as for Configuration 1.

The general remarks concerning the radial traverse data and static pressure distributions on the annulus walls are essentially the same for Configuration 2 as for Configuration 1. The difference in performance between these two configurations are discussed in Sect. 4.2.

4.2 COMPARISON BETWEEN ROTORS

The performance of the first and second configurations of Rotor 1 is compared over the entire speed range but in detail only at design speed. The compressor maps of the two configurations are superposed in Figs. 4 and 5 for 60-, 80-, and 100-percent design speed. At design speed, very little difference in performance is observed in total pressure ratio, isentropic efficiency, or mass flow. The effect of opening up the rotor flow passage, according to Ref. 3, was supposed to be an increase in rotor diffusion, thereby a decrease in dumping losses and an increase in pressure ratio and efficiency. The increased performance was expected only if boundary-layer blockage in the rotor did not increase a corresponding amount. From the experimental compressor

maps, it appears that blockage increased in nearly exact proportion to the increase in passage area because no improvement was observed. This is discussed in Sect. V.

At lower speeds, the second configuration choked at a higher value of mass flow than the first configuration. Since the effect of boundary-layer blockage and flow separation decrease with decreasing back pressure and rotor speed, the increase in flow with the second configuration is logical. As speed was reduced from 100 to 80 percent, the stalling value of total pressure ratio and of efficiency achieved with the second configuration dropped below those values achieved with the first. However, as speed decreased further to 60 percent and below, the stalling total pressure ratio of the second configuration recovered to that of the first and the peak efficiency exceeded that of the first. It appears that at supersonic and transonic speeds, the rotor boundary layers were not capable of sustaining the additional diffusion demanded by the greater blade-passage divergence of the second configuration. At subsonic speeds, the diffusion was evidently not excessive and the performance benefited because of the reduced velocity arriving at the abrupt trailing-edge diffusion zone. However, the range of flow between stall and choke was reduced for the second configuration at all speeds below design speed.

The annulus wall static pressure distribution measured at design speed and maximum back pressure is shown for each configuration, superposed in Fig. 6. The distribution has the same character for both configurations, although a slightly higher static pressure level is noted for Configuration 2. However, the higher static pressure rise experienced with the second configuration does not appear to be due to the higher over-all diffusion expected, since mass-averaged performance at this point was virtually unchanged. Rather, it seems to reflect a change in the radial distribution of the flow, which was less distorted with Configuration 2, having more diffusion near the tip and less diffusion near the hub. The dip in static pressure just downstream of the rotor is evident for both configurations. As mentioned in Ref. 3, this is characteristic of a local zone of boundary-layer separation on the casing wall.

Radial distributions of various parameters, measured 2 in. downstream of the rotor at design speed, and maximum back pressure, are superposed for the two configurations in Figs. 7 through 12. The differences in performance between the two configurations are slight. However, the uniformity of all plotted quantities was somewhat better with Configuration 2. A drastic fall-off in specific mass flow is evident for both configurations in the outer 50 percent of the annulus. This is probably attributable to the casing boundary-layer separation bubble which is located between the 2-in. downstream measuring station and the rotor. The corresponding absolute flow angle also increases sharply in this same zone.

SECTION V
CONCLUSIONS

The major conclusion to be drawn from these two experiments is that the configurations tested demanded too much diffusion for either the rotor or the downstream diffusion zone to handle efficiently. Although the blunt trailing edges limited diffusion within the blade row, the lack of any annulus convergence caused a very rapid diffusion and subsequent boundary-layer separation downstream.

A second conclusion may be drawn from the observation that the modification of Configuration 1 to produce Configuration 2 (namely, increasing rotor flow passage divergence) does not lead to an increase in performance. The mathematical model presented in Ref. 3 showed that, if boundary-layer blockage within the blade row did not increase, more diffusion should take place within the blade row. Thus, the losses leaving the blade row would be reduced, causing an overall increase in performance. Since this did not occur, and since stall occurred at nearly the same pressure ratios as before, it might be concluded that the blockage term employed in the theory does not really represent boundary-layer blockage but indicates the size of the separation zone between blades. The flow is expected to separate on the suction surface of each blade, at or near design speed, where the bow shock of each adjacent blade impinges. If little or no reattachment takes place, opening up the passage may produce virtually no change in the fluid mainstream and only move the free surface of the fluid a corresponding amount further away from the suction surface of each blade.

At subsonic speeds, 60-percent design for example, efficiency was increased at the expense of flow range, and stalling pressure ratio remained about the same. It may be concluded for this condition that separation was no longer a factor before the stall point was reached and that the increased divergence of the passage did produce increased rotor diffusion, leading to equivalent pressure ratios at higher mass flows.

REFERENCES

1. Johnson, E. G., von Ohain, H., Lawson, M. D., and Cramer, K. R. "A Blunt-Trailing-Edge Supersonic Compressor Blading." WADC TN 59-269, 1959.

2. Chauvin, J. "The Concept of Blunt-Trailing-Edge Blading for Use in Supersonic Compressors." Paper DK 533-697-242-011.5, Jahrbuch 1962 der WFLR, Vieweg and Sohn, Braunschweig, Germany, 1963.

3. Wennerstrom, A. J. and Olympios, S. "A Theoretical Analysis of the Blunt-Trailing-Edge Supersonic Compressor and Comparison with Experiment." ARL 66-0236, 1966.

4. Chauvin, J. "Research on the Concept of Blunt-Trailing-Edge Blades," von Karman Institute for Fluid Dynamics, Rhode St.-Genese, Belgium, 1965.

5. Carman, C. T. "Development of the Supersonic Compressor Test Facilities at the Arnold Engineering Development Center." AEDC-TR-65-169 (AD 471021), 1965.

APPENDIXES

I. ILLUSTRATIONS
II. METHODS OF CALCULATION
III. MEASUREMENT UNCERTAINTY
IV. DATA SUMMARY FOR CONFIGURATIONS 1 AND 2

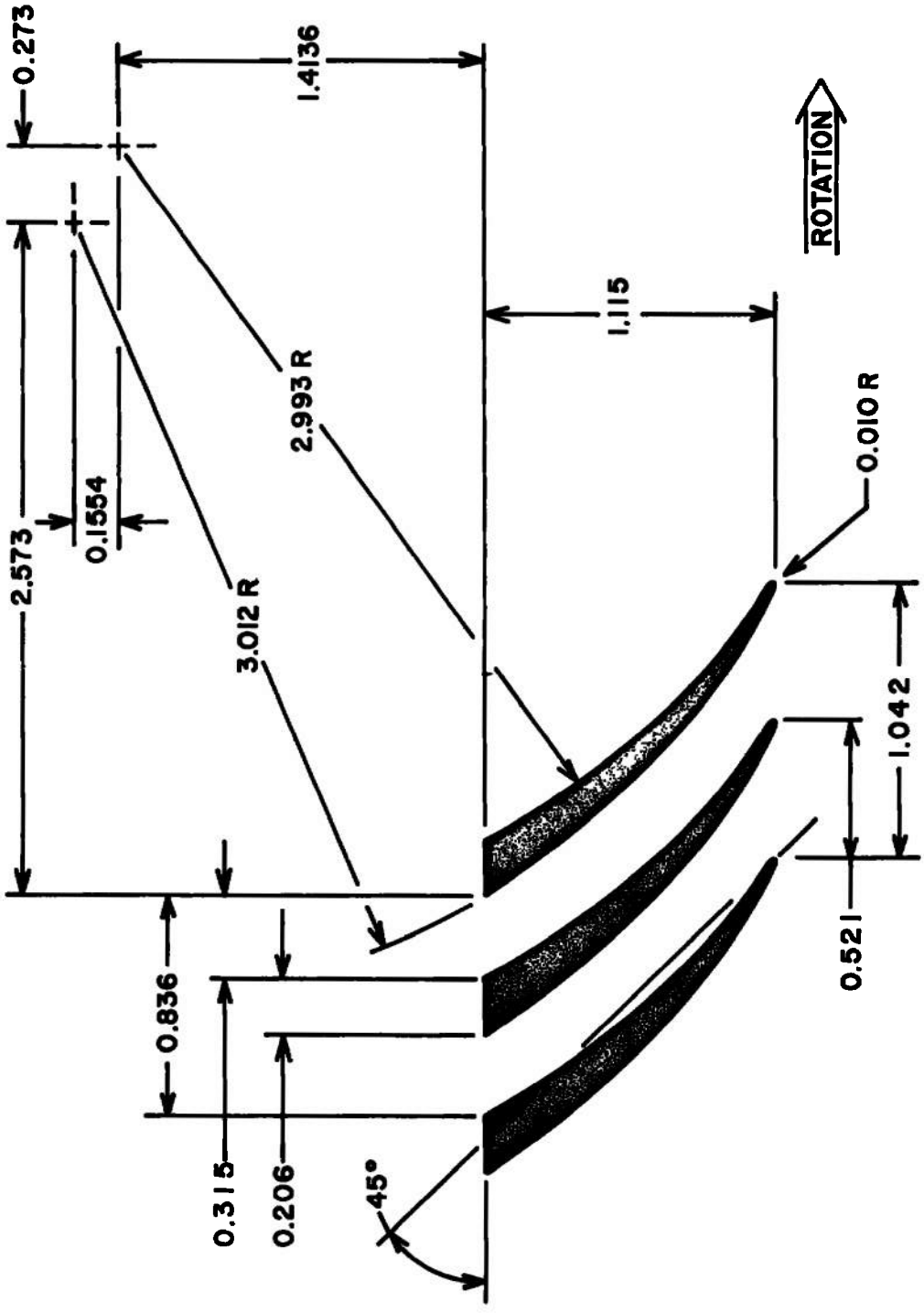

a. Blunt-Trailing-Edge Blade Configuration 1

Fig. 1 Blade Geometry of Mean Radius Profile

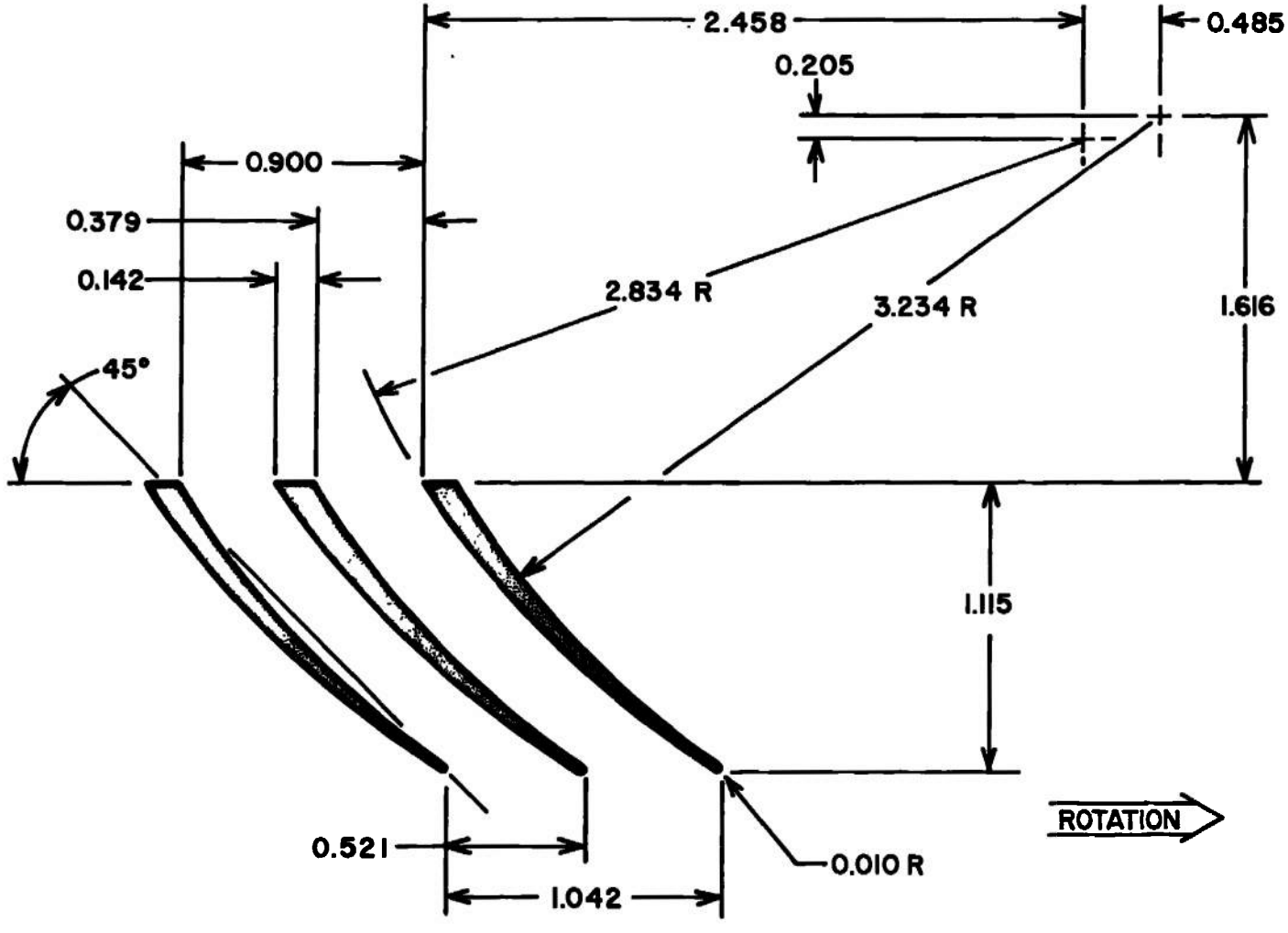

b. Blunt-Trailing-Edge Blade Configuration 2

Fig. 1 Concluded

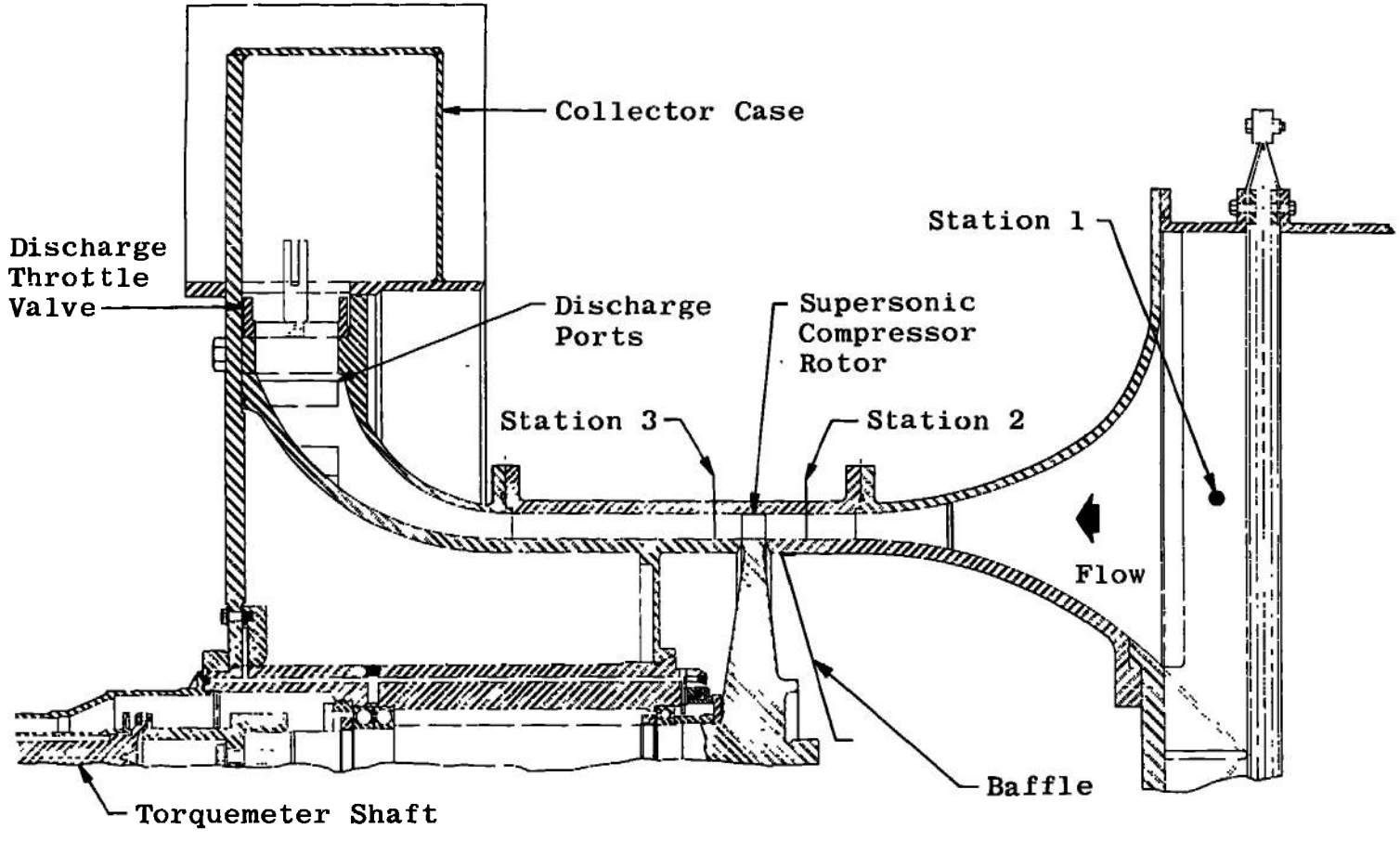

Fig. 2 Cross-Sectional View of Experimental Compressor

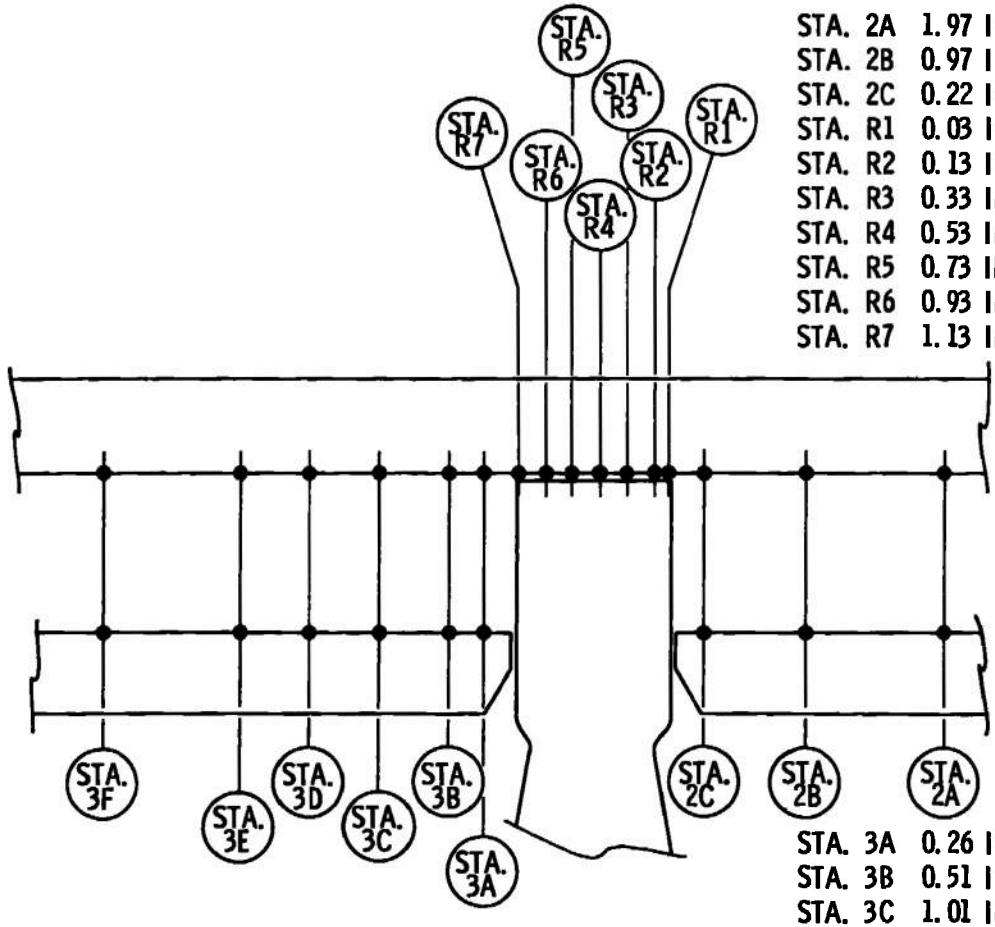

• WALL STATIC PRESSURE TAPS

STA. 2A	1.97 IN.	FORWARD OF LEADING EDGE
STA. 2B	0.97 IN.	" " "
STA. 2C	0.22 IN.	" " "
STA. R1	0.03 IN.	BEHIND LEADING EDGE
STA. R2	0.13 IN.	" " "
STA. R3	0.33 IN.	" " "
STA. R4	0.53 IN.	" " "
STA. R5	0.73 IN.	" " "
STA. R6	0.93 IN.	" " "
STA. R7	1.13 IN.	" " "

STA. 3A	0.26 IN.	BEHIND TRAILING EDGE
STA. 3B	0.51 IN.	" " "
STA. 3C	1.01 IN.	" " "
STA. 3D	1.51 IN.	" " "
STA. 3E	2.01 IN.	" " "
STA. 3F	3.01 IN.	" " "

a. Station Locations

Fig. 3 Details of Instrumentation Stations

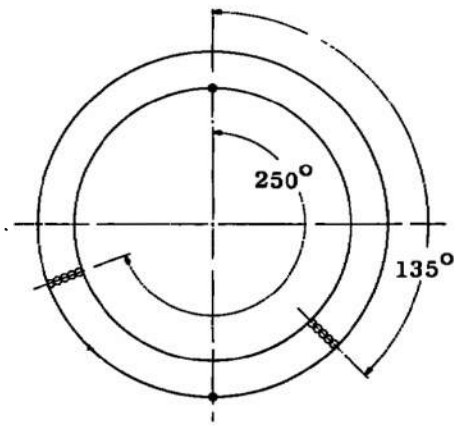

b. Station 2A

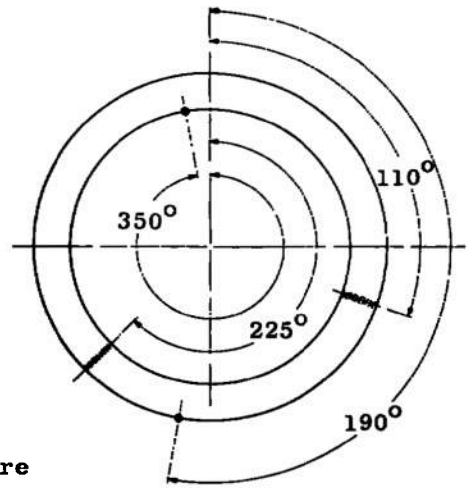

c. Station 2B

∘ Total Pressure
• Static Pressure
x Total Temperature
Traverse
Yaw Angle

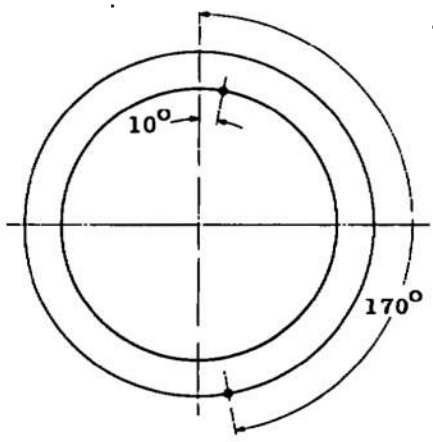

d. Station 2C

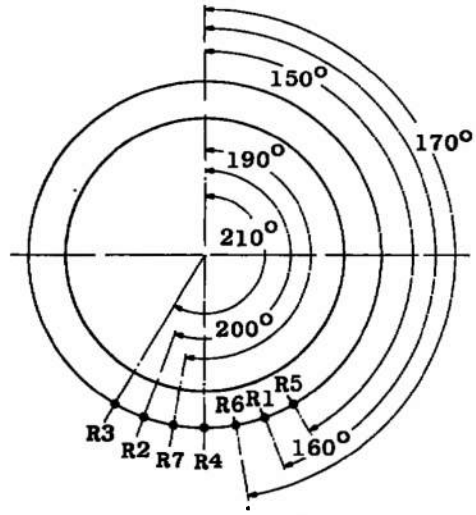

e. Station R1 – R7

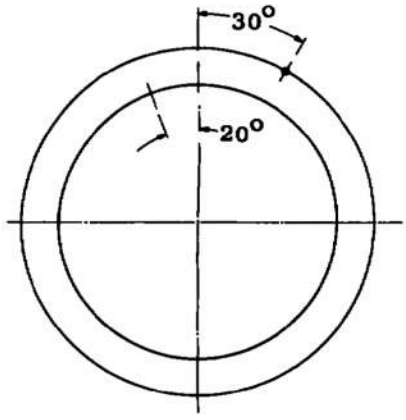

f. Station 3A

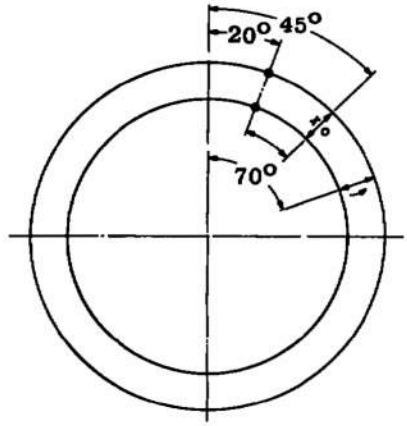

g. Station 3B

Fig. 3 Continued

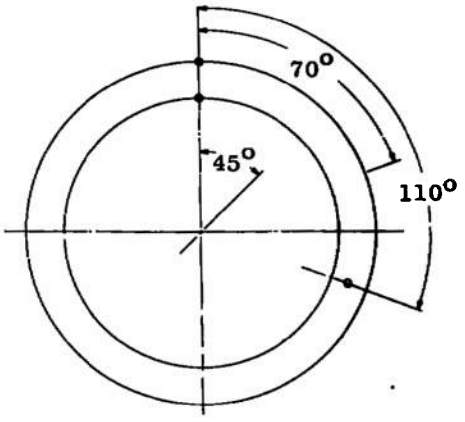

h. Station 3C

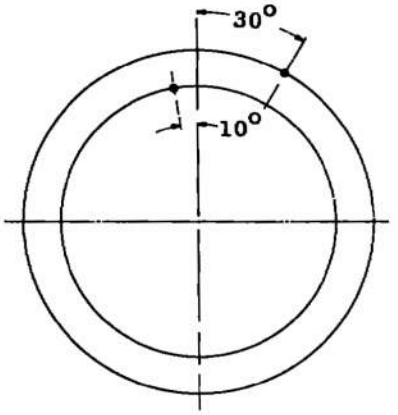

i. Station 3D

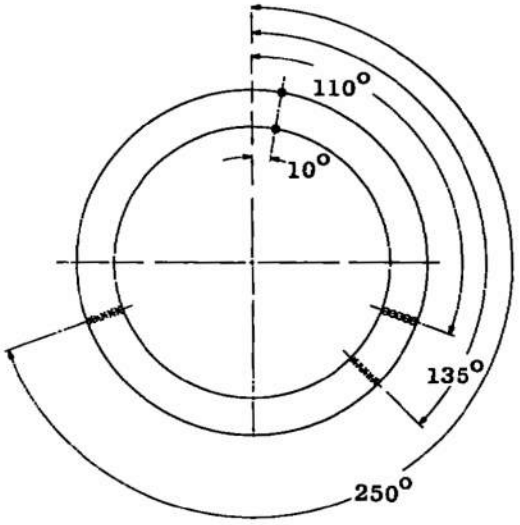

j. Station 3E

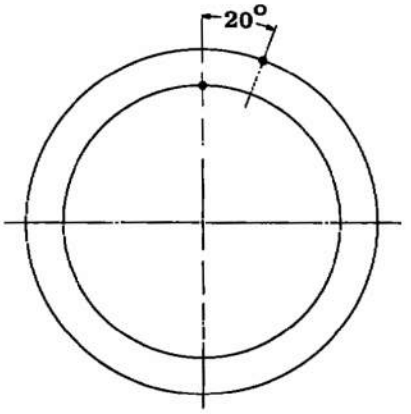

k. Station 3F

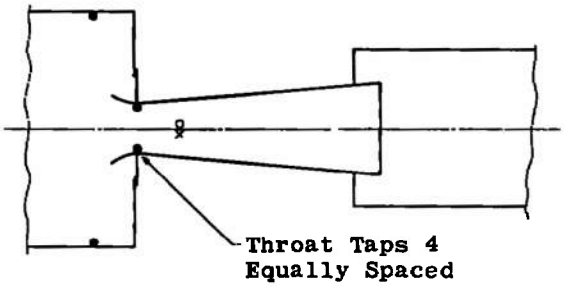

l. Venturi Instrumentation

Fig. 3 Concluded

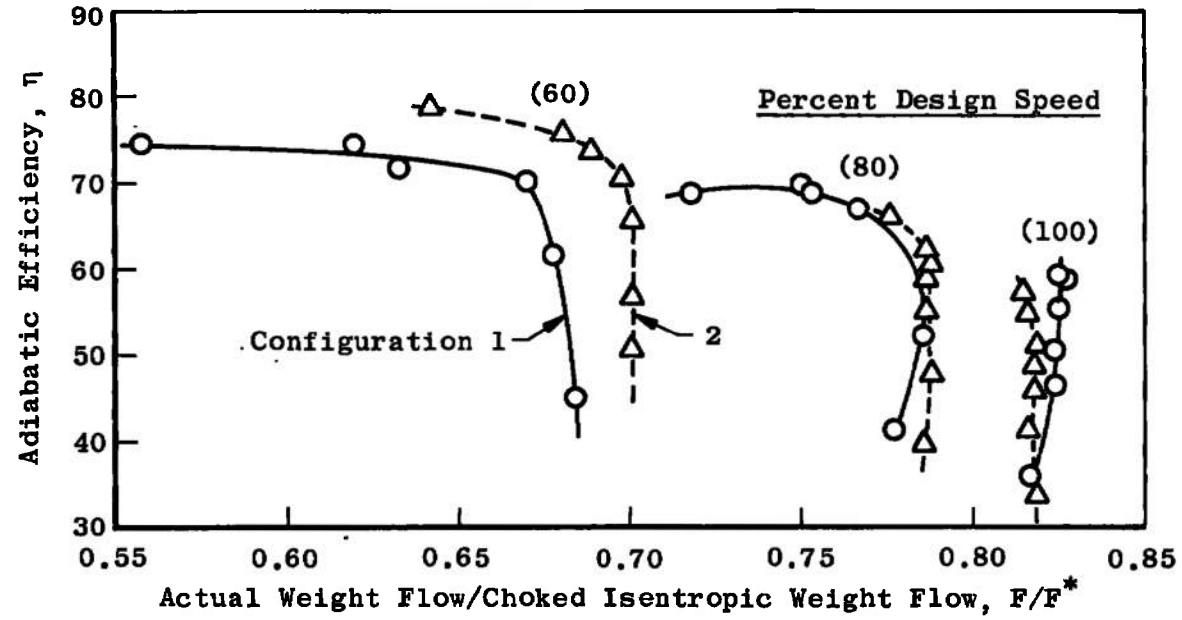

Fig. 4 Rotor Isentropic Efficiency

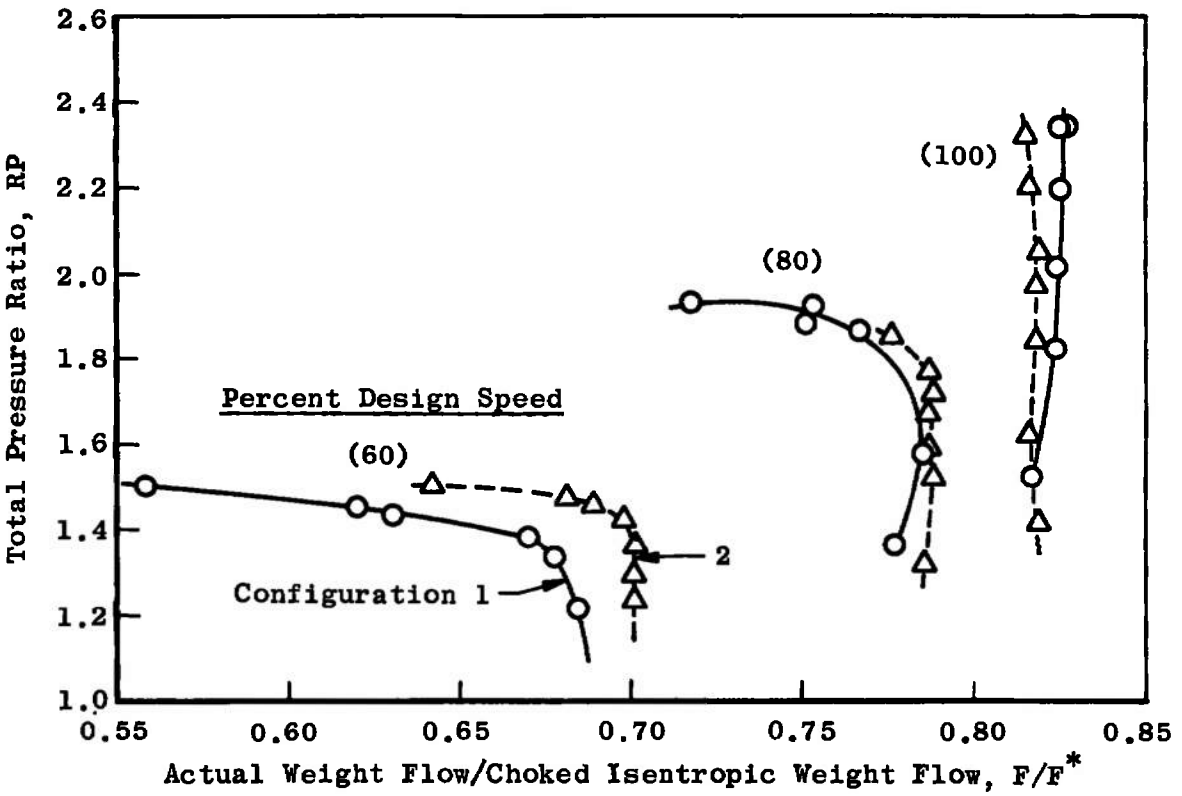

Fig. 5 Rotor Total Pressure Ratio

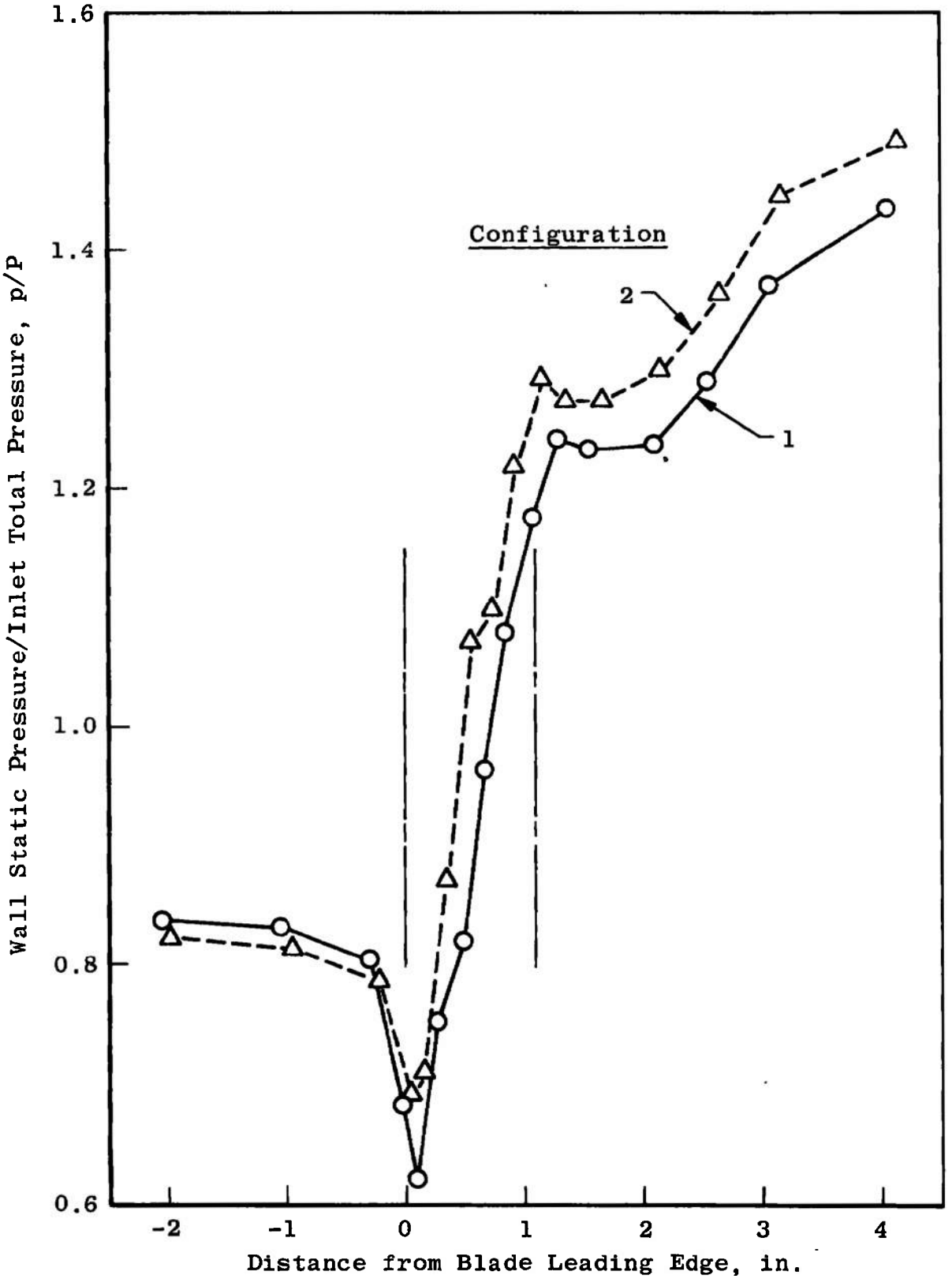

Fig. 6 Casing Static Pressure Distribution at Design Speed and Maximum Back Pressure

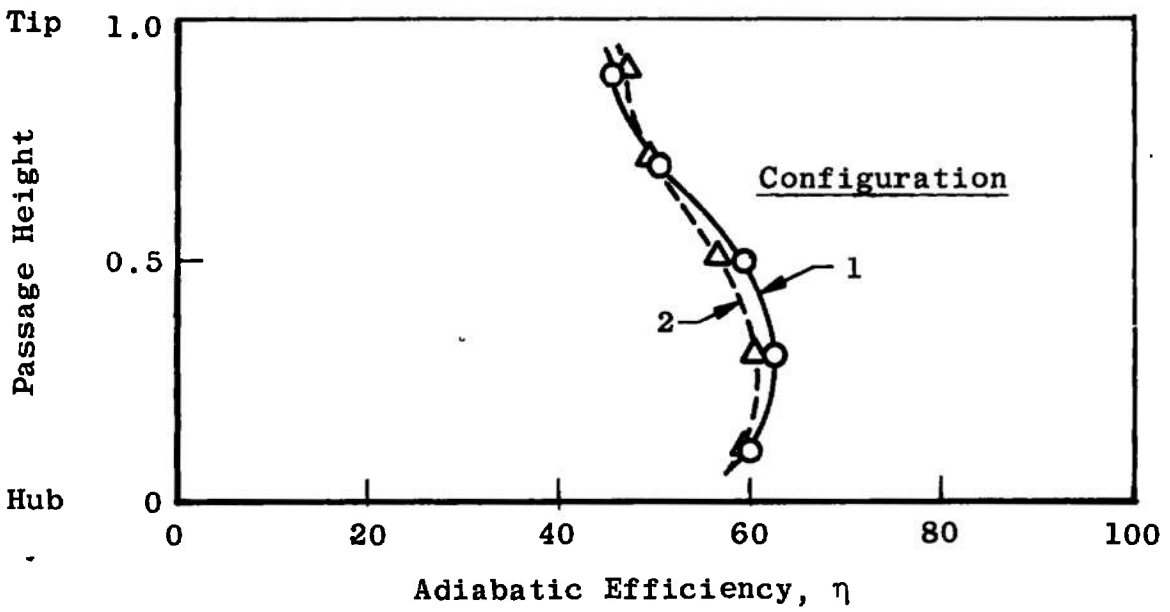

Fig. 7 Efficiency Distribution at Design Speed and Maximum Back Pressure

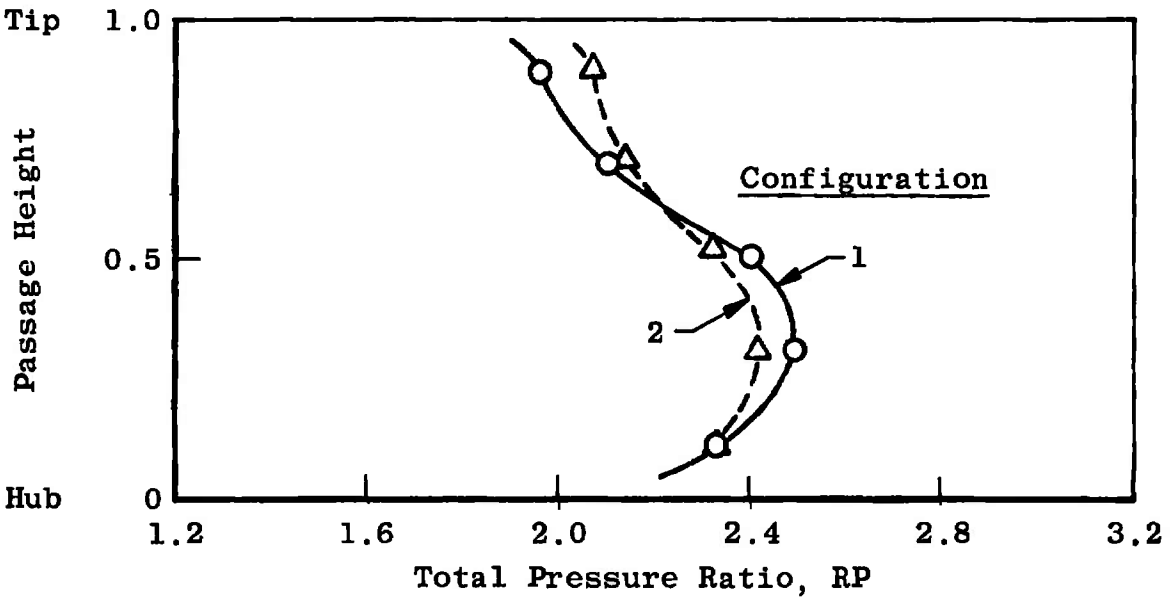

Fig. 8 Total Pressure Distribution at Design Speed and Maximum Back Pressure

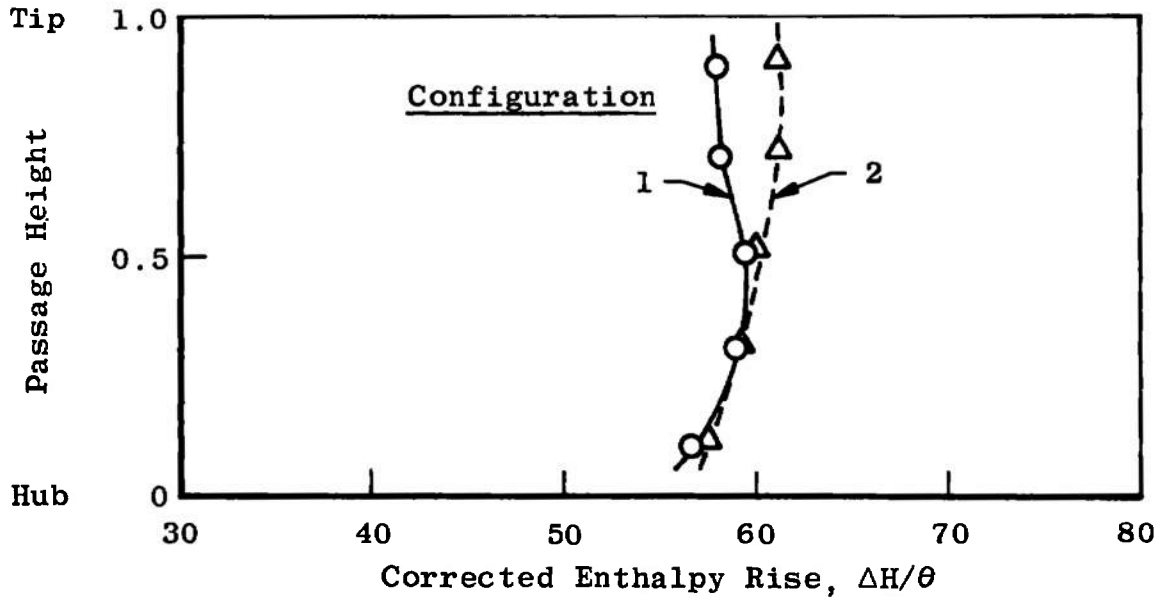

Fig. 9 Corrected Enthalpy Rise at Design Speed and Maximum Back Pressure

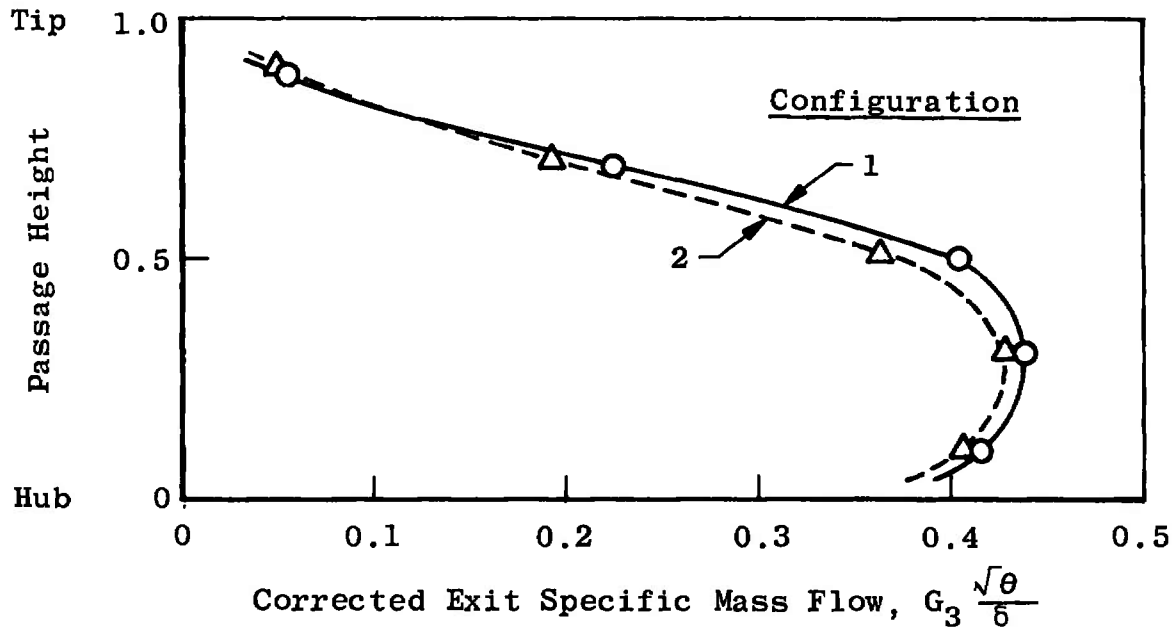

Fig. 10 Specific Mass Flow Distribution at Design Speed and Maximum Back Pressure

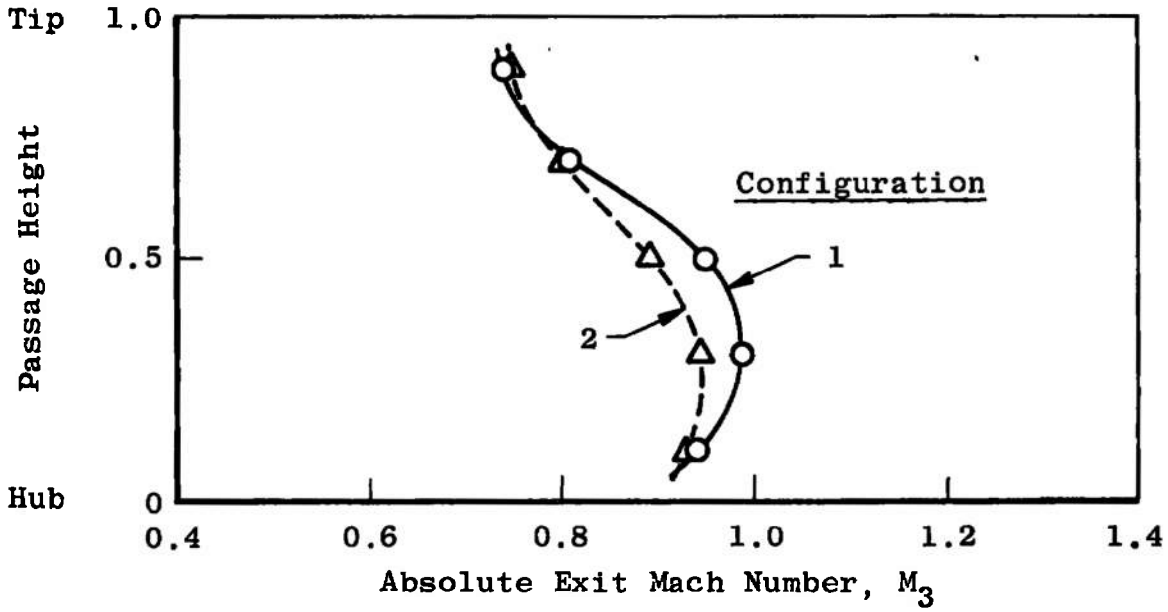

Fig. 11 Absolute Exit Mach Number Distribution at Design Speed and Maximum Back Pressure

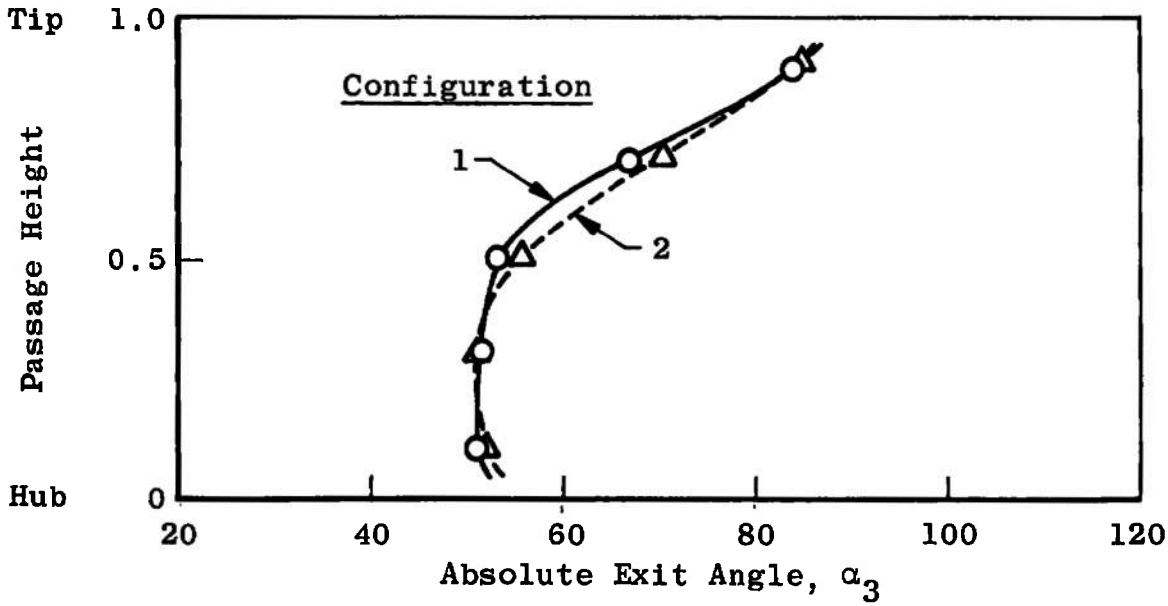

Fig. 12 Absolute Exit Flow Angle Distribution at Design Speed and Maximum Back Pressure

APPENDIX II
METHODS OF CALCULATION

General methods and equations employed to compute the parameters presented are given herein. Test data were processed to the final parameters with an IBM 360/50 digital computer.

TEMPERATURE

Discharge total temperatures were corrected by applying a recovery factor of 0.96 to the indicated temperature measurements in the calculation:

$$T_3 = \frac{T_i(\gamma M^2 - M^2 + 2)}{RF(\gamma M^2 - M^2) + 2}$$

Static temperatures were calculated from the measured stagnation temperatures and pressures by using perfect gas, isentropic relations:

$$t = T\left(\frac{p}{P}\right)^{\frac{\gamma-1}{\gamma}}$$

The static pressure values across the passage were assumed as a linear variation from the measured static pressures at the walls.

SPECIFIC HEAT

The specific heat at constant pressure was computed from the empirical equation:

$$C_p = 0.2318 + 0.104 \times 10^{-4} T + 0.7166 \times 10^{-8} T^2$$

The ratio of specific heats was assumed to be 1.4 at the venturi and inlet stations. At all other stations the ratio of specific heats was calculated from the expression

$$\gamma = \frac{C_p}{C_p - \frac{R}{J}}$$

When applicable, arithmetic averages of the specific heat ratios were used.

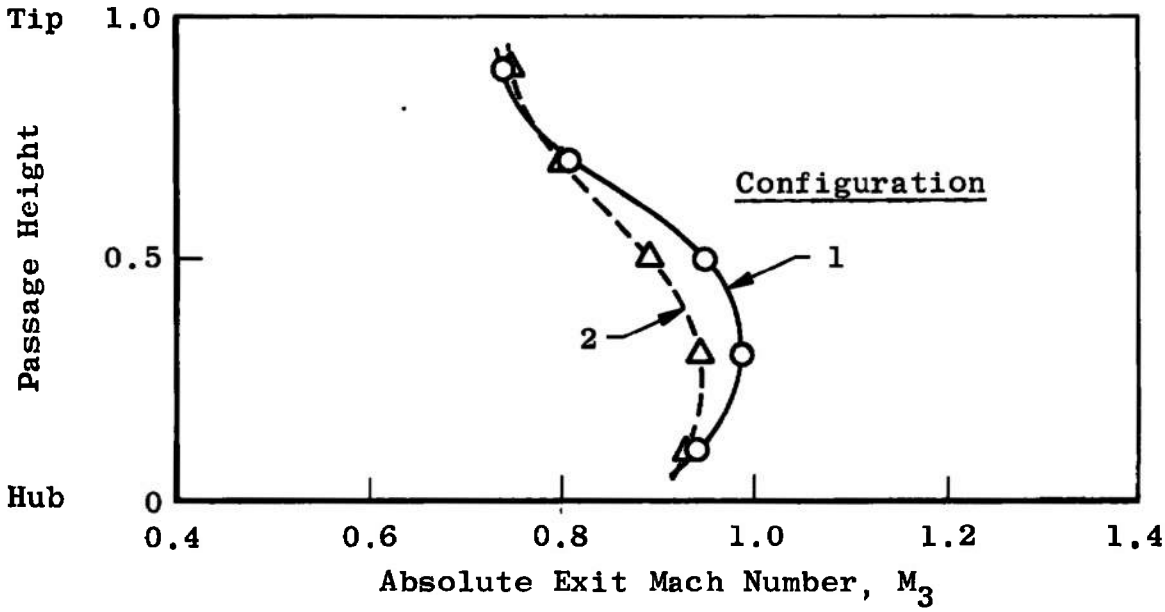

Fig. 11 Absolute Exit Mach Number Distribution at Design Speed and Maximum Back Pressure

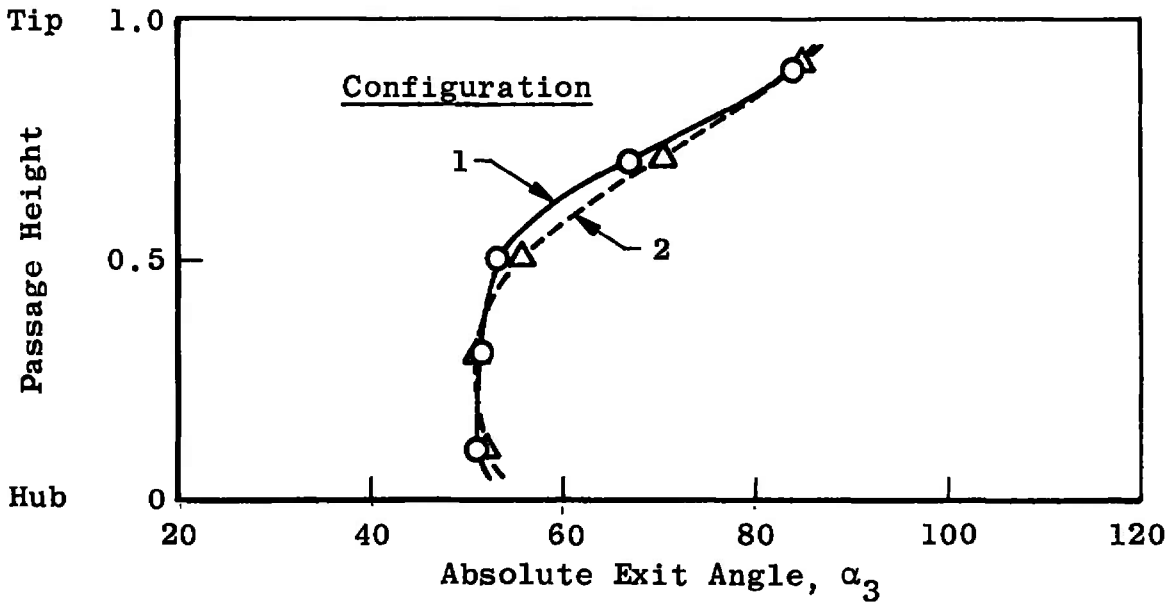

Fig. 12 Absolute Exit Flow Angle Distribution at Design Speed and Maximum Back Pressure

APPENDIX II
METHODS OF CALCULATION

General methods and equations employed to compute the parameters presented are given herein. Test data were processed to the final parameters with an IBM 360/50 digital computer.

TEMPERATURE

Discharge total temperatures were corrected by applying a recovery factor of 0.96 to the indicated temperature measurements in the calculation:

$$T_3 = \frac{T_i(\gamma M^2 - M^2 + 2)}{RF(\gamma M^2 - M^2) + 2}$$

Static temperatures were calculated from the measured stagnation temperatures and pressures by using perfect gas, isentropic relations:

$$t = T\left(\frac{p}{P}\right)^{\frac{\gamma-1}{\gamma}}$$

The static pressure values across the passage were assumed as a linear variation from the measured static pressures at the walls.

SPECIFIC HEAT

The specific heat at constant pressure was computed from the empirical equation:

$$C_p = 0.2318 + 0.104 \times 10^{-4} T + 0.7166 \times 10^{-8} T^2$$

The ratio of specific heats was assumed to be 1.4 at the venturi and inlet stations. At all other stations the ratio of specific heats was calculated from the expression

$$\gamma = \frac{C_p}{C_p - \frac{R}{J}}$$

When applicable, arithmetic averages of the specific heat ratios were used.

AIRFLOW

Airflow was calculated at the venturi from the following equation using a flow coefficient (C_f) of 0.99:

$$F = C_f AP \left[\frac{2\gamma g}{RT(\gamma - 1)} \left(\left[\frac{p}{P} \right]^{\frac{2}{\gamma}} - \left[\frac{p}{P} \right]^{\frac{\gamma + 1}{\gamma}} \right) \right]^{1/2}$$

ABSOLUTE MACH NUMBER

Mach number was obtained from the compressible flow equation:

$$M = \left(\frac{2}{\gamma - 1} \right)^{1/2} \left[\left(\frac{P}{p} \right)^{\frac{\gamma - 1}{\gamma}} - 1 \right]^{1/2}$$

ADIABATIC EFFICIENCY

The adiabatic efficiency was computed from the following expressions:

$$\eta = \frac{\Delta H_{ideal}}{\Delta H_{actual}}$$

where

$$\Delta H = \int_{T_2}^{T_3} C_p \, dT$$

$$\text{Ideal } T_3 = T_2 \left(\frac{P3}{P2} \right)^{\frac{\gamma - 1}{\gamma}}$$

$$\text{Actual } T_3 = T_3 \text{ measured}$$

VELOCITY

Velocity was determined from the expression:

$$C = \left(\frac{2\gamma Rgt}{\gamma - 1} \right)^{1/2} \left[1 - \left(\frac{p}{P} \right)^{\frac{\gamma - 1}{\gamma}} \right]^{1/2}$$

RELATIVE FLOW ANGLE

Relative flow angle to the blade was obtained by

$$\beta = \arctan \frac{U - C \sin \alpha}{C \cos \alpha}$$

where

$$U = \frac{2\pi}{60} r N$$

RELATIVE MACH NUMBER

Relative Mach number to the blade was determined by

$$M_w = \frac{\frac{W}{C}}{M}$$

where

$$W = \frac{U - C \sin \alpha}{\sin \beta}$$

MASS-WEIGHTING FACTOR

Specific mass flow is used as a weighting factor in the summation of various parameters computed from data measured in the five equal areas across the annulus passage and is calculated by

$$G = pM \left(\frac{g\gamma}{RT} \right)^{1/2} \cos \alpha$$

APPENDIX III
MEASUREMENT UNCERTAINTY

Physical measurements involve two basic classes of error - precision or repeatability error and accuracy error. Precision error is present when successive measurements of an unchanged quantity yield different numerical results. Accuracy error is present when the numerical average of successive readings deviates from the known correct reading and continues to do so no matter how many successive readings are taken.

Accuracy error is eliminated by calibration. The total pressure probes have been calibrated aerodynamically. Total temperature probes have been calibrated in an oil bath (see references).

Without a great many replications of readings with the entire measurement system, precision error can only be estimated from manufacturers' specifications for each component of the system. Tables III-I and III-II show the estimated precision for the instrumentation of, respectively, configurations 1 and 2. In these tables the system sensor implies the transducer in the case of pressure measurements and the thermocouple junction for the temperature measurements. Transmission error for temperature measurements depends on the wire used. Reference errors may involve the accuracy in reading atmospheric pressure or some base reference. Read-out error includes both interpretation and digitizing error. The total precision is the arithmetic sum of these values. If calibration has been used to eliminate accuracy error, these figures represent the total uncertainty of a single measurement.

The final column of Tables III-I and III-II presents the number of times a single point is replicated. Traverse measurements are manually read while rake data are electronically recorded. During one traverse there is time to make three complete scans of rake data. Since error in an average is inversely proportional to the square of the number of readings making up the average,[1] it is felt that the rake measurements probably represent the more accurate values.

The precision index W_R of a general function R where

$$R = f(x_1, x_2, \cdots x_n)$$

may be calculated by

$$W_R = \left[\sum_{i=1}^{n} \left(\frac{\partial R}{\partial x_i} \right)^2 W_i^2 \right]^{1/2}$$

[1]Hilbert, Shenck, Jr. Theories of Engineering Experimentation. McGraw-Hill Book Company, New York, N. Y., 1961.

where W_i is the prevision of the independent variables. Using this relation and the estimated precision of Tables III-I and III-II and assuming constant specific heat at constant pressure, the estimated precision in total pressure ratio, RP, adiabatic efficiency, η, inlet absolute Mach number, M_2, and outlet absolute Mach number, M_3, is calculated at the extremes of operating conditions. Inlet stagnation conditions are assumed standard.

The following table summarizes the results of the computation where the precisions indicated represent approximately twice the standard deviation.

CONFIGURATION I

	W_{RP}	W_N	W_{M_2}	W_{M_3}
1.0N Max	± 0.021	± 0.017	± 0.004	± 0.001
0.5N Min	± 0.013	± 0.088	± 0.005	± 0.004

CONFIGURATION 2

	W_{RP}	W_N	W_{M_2}	W_{M_2}
1.0N Max	± 0.014	± 0.015	± 0.002	± 0.001
0.5N Min	± 0.011	± 0.072	± 0.002	± 0.004

The apparent large uncertainty in efficiency at low-speed operation is not born out in repeated measurements near this condition. Precision in efficiency based on seven data points at 0.6N minimum pressure ratio is computed to be approximately ± 0.020.

Mass flow is measured by a venturi flowmeter with manometer board pressure measurements photographically recorded and temperature measurements recorded electronically. The precision of the mass flow measurements at 1.0N maximum pressure ratio is computed to be approximately ± 0.415 lb_m/sec. This value includes allowance for error in readings of atmospheric pressure and fluid column heights; fluid density change caused by variation in ambient temperature and manometer board temperature gradients; sensor, transmission, reference and read-out errors in temperature; round-off errors in millivolt to Fahrenheit degree conversion; venturi throat area measurement precision; and the flow coefficient.

Rpm is measured by a frequency counter for the output of an electromagnetic pickup. The accuracy is ±1 count digitizing error, ±0.04 percent of the reading caused by scale conversion, ±10 counts error in reading during operation. At maximum rpm this amounts to ±0.1 percent error.

TABLE III-I
CONFIGURATION 1

PARAMETER	SENSOR PRECISION	TRANSMISSION PRECISION	REFERENCE PRECISION	READ-OUT PRECISION	TOTAL PRECISION	REPETITION
Total Pressure						
Inlet Rake	±0.100 psi		±0.005 psi	±0.015 psi	±0.120 psi	6
Outlet Rake	±0.125 psi			±0.015 psi	±0.140 psi	3
Outlet Traverse	±0.125 psi			±0.125 psi	±0.250 psi	
Static Pressure						
Inlet Wall 2A, 2B, 2C	±0.100 psi		±0.005 psi	±0.015 psi	±0.120 psi	3
Wheel Wall						
TR1, 2, 3, 4	±0.100 psi		±0.005 psi	±0.015 psi	±0.120 psi	3
TR5, 6, 7	±0.500 psi		±0.005 psi	±0.015 psi	±0.520 psi	3
Outlet Wall						
3A, 3B, 3E, 3F	±0.125 psi			±0.015 psi	±0.140 psi	3
3C, 3D	±0.500 psi		±0.005 psi	±0.015 psi	±0.520 psi	3
Total Temperature						
Inlet Rake	±1°R	±2.0°R	±0.200°R	±0.006MV(0.324°R)	±3.524°R	6
Outlet Rake	±1°R	±2.0°R	±0.200°R	±0.006MV(0.324°R)	±3.524°R	6
Outlet Traverse	±1°R	±2.0°R	±0.875°R	±1.0°R	±4.875°R	1
Absolute Flow Angle	±0.25 deg		±0.50 deg	±0.50 deg	±1.25 deg	1

TABLE III-II
CONFIGURATION 2

PARAMETER	SENSOR PRECISION	TRANSMISSION PRECISION	REFERENCE PRECISION	READ-OUT PRECISION	TOTAL PRECISION	REPETITION
Total Pressure						
Inlet Rake	±0.050 psi			±0.015 psi	±0.065 psi	6
Outlet Rake	±0.125 psi			±0.015 psi	±0.140 psi	3
Outlet Traverse	±0.125 psi			±0.125 psi	±0.250 psi	1
Static Pressure						
Inlet Wall 2A, 2B, 2C	±0.050 psi			±0.015 psi	±0.065 psi	3
Wheel Wall TR1, 2, 3	±0.050 psi			±0.015 psi	±0.065 psi	3
TR4	±0.075 psi			±0.015 psi	±0.090 psi	3
TR5, 6, 7	±0.500 psi		±0.005 psi	±0.015 psi	±0.520 psi	3
Outlet Wall 3A, 3B, 3E, 3F	±0.125 psi			±0.015 psi	±0.140 psi	3
3C, 3D	±0.500 psi		±0.005 psi	±0.015 psi	±0.520 psi	3
Total Temperature						
Inlet Rake	±1°R	±2.0°R	±0.200°R	±0.006MV(0.324°R)	±3.524°R	6
Outlet Rake	±1°R	±2.0°R	±0.200°R	±0.006MV(0.324°R)	±3.524°R	6
Outlet Traverse	±1°R	±2.0°R	±0.875°R	±1.0°R	±4.875°R	1
Absolute Flow Angle	±0.25 deg		±0.50 deg	±0.50 deg	±1.25 deg	1

APPENDIX IV
DATA SUMMARY FOR CONFIGURATIONS 1 AND 2

ILLUSTRATIONS

TABLES

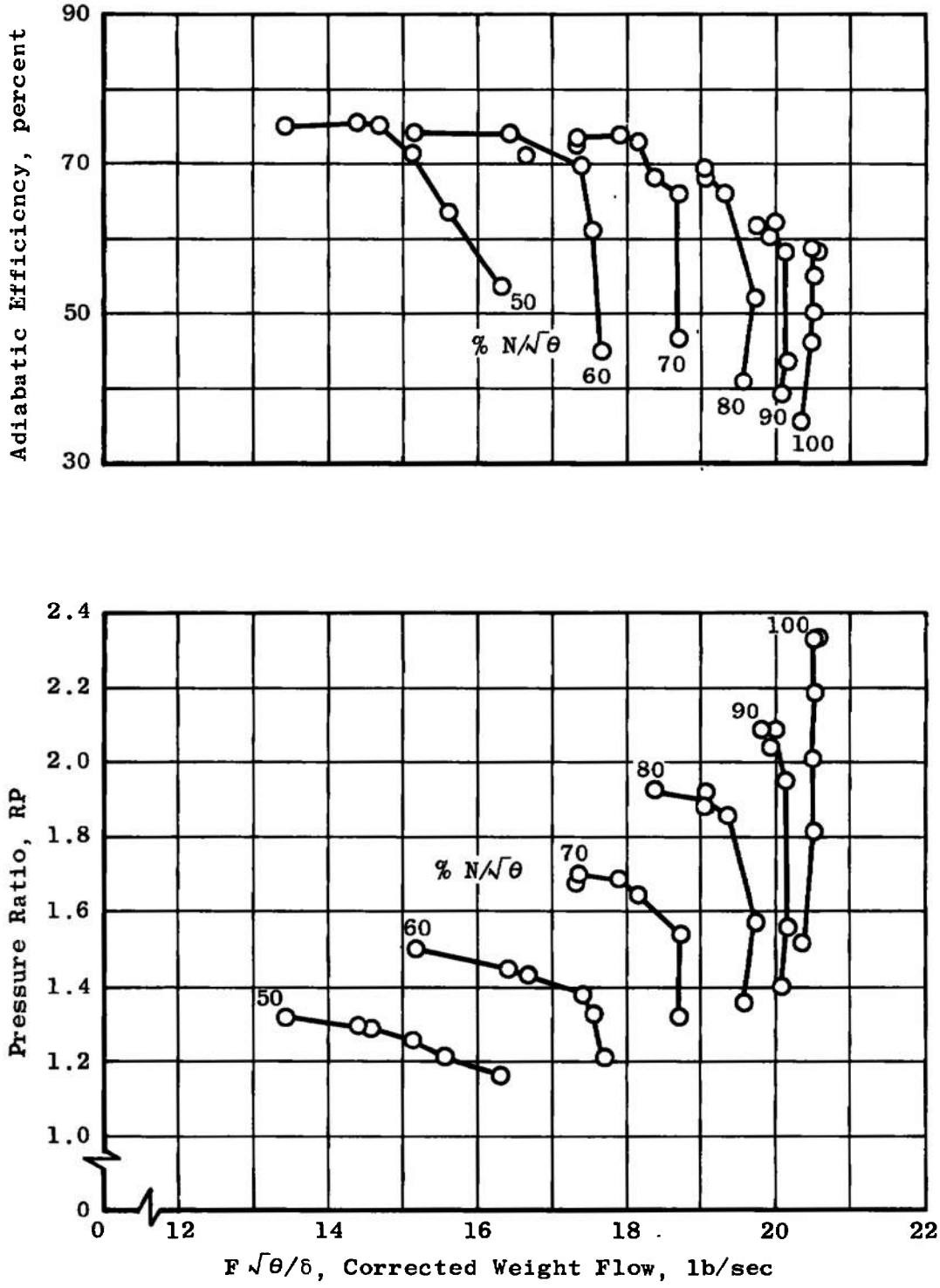

a. Compressor Performance Characteristics Based on Equivalent Weight Flow

Fig. IV-1 Configuration 1

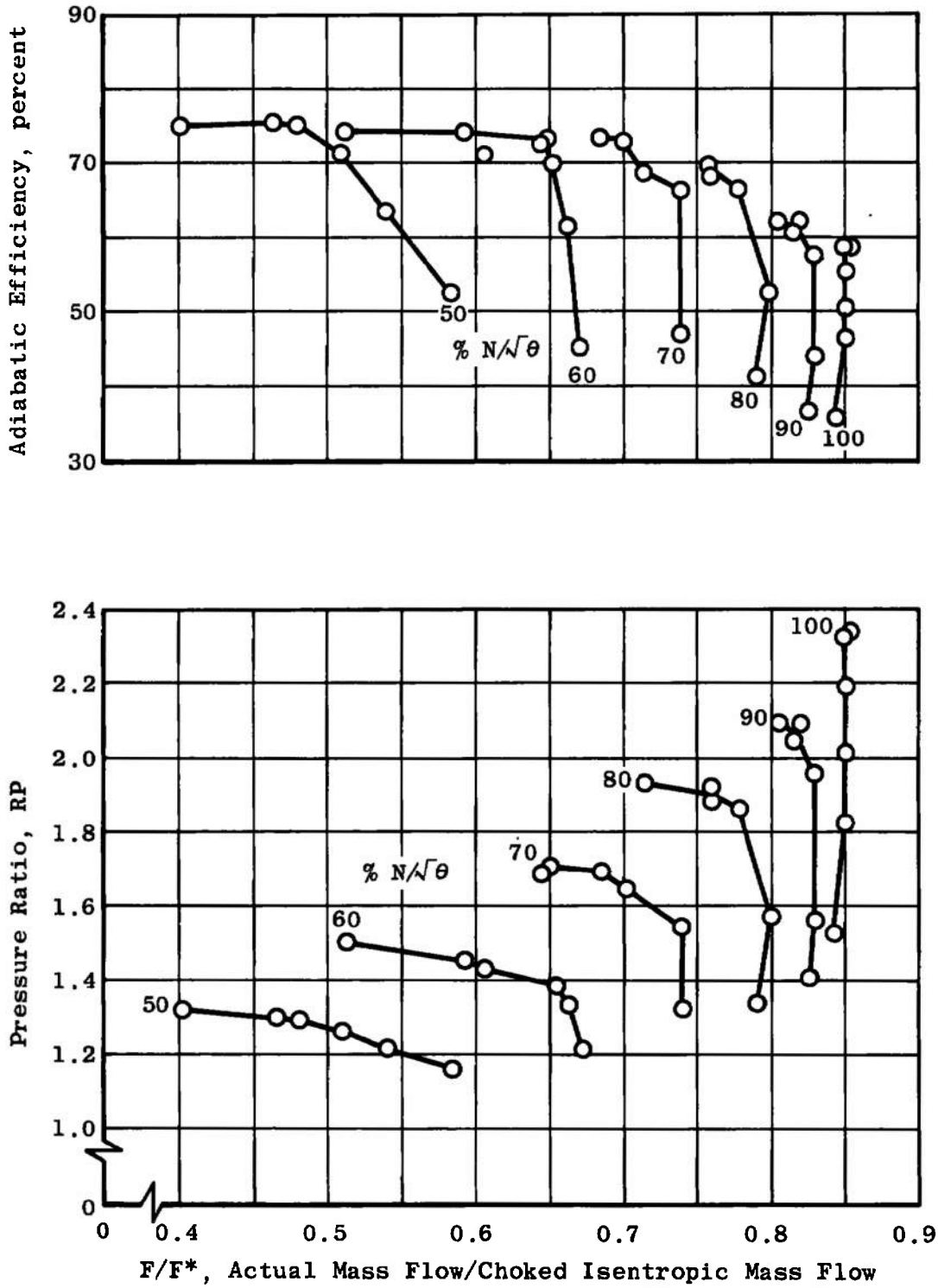

b. Compressor Performance Characteristics Based on Weight Flow Ratio

Fig. IV-1 Continued

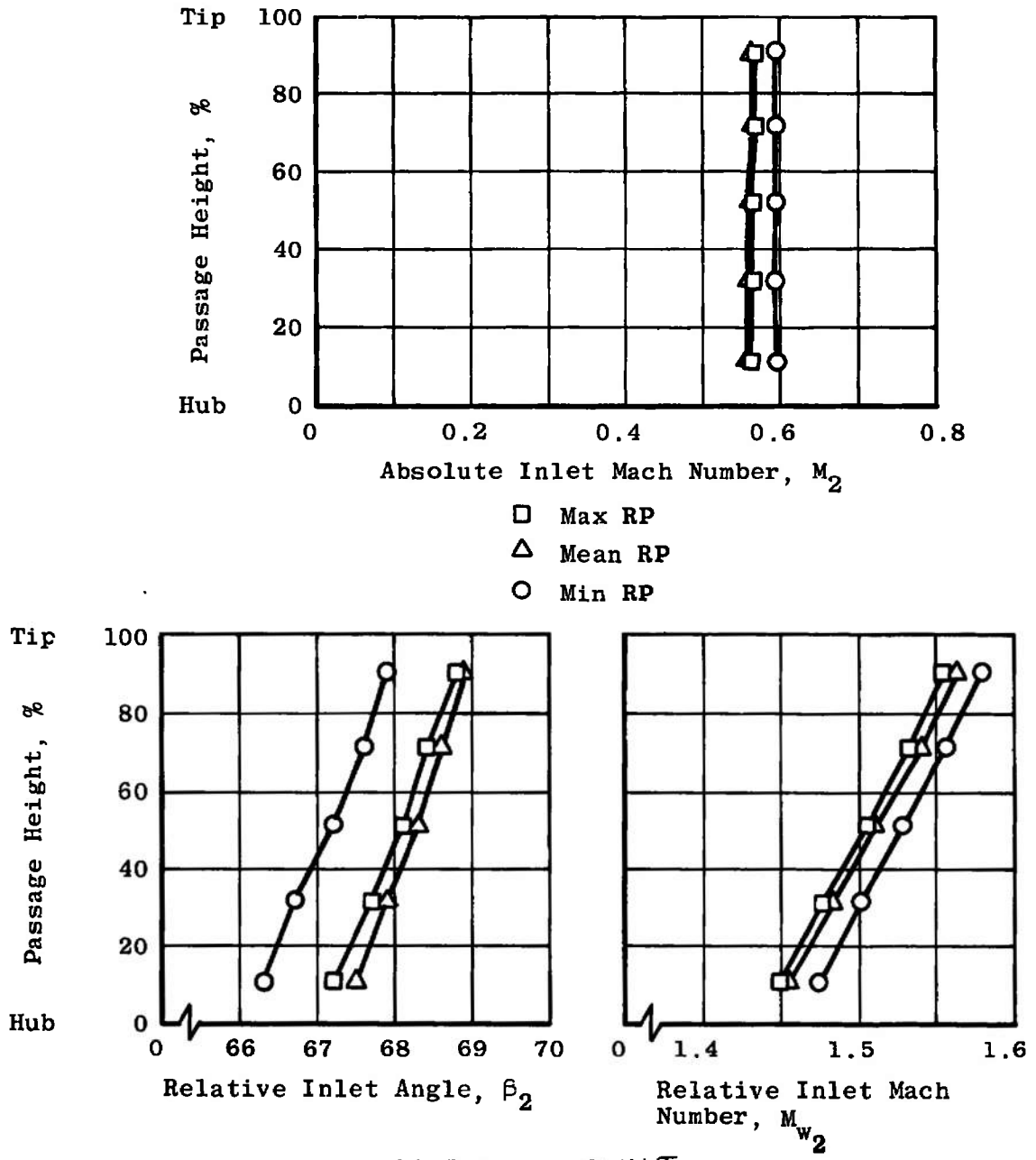

c. Inlet Parameters, 100% $N/\sqrt{\theta}$

Fig. IV-1 Continued

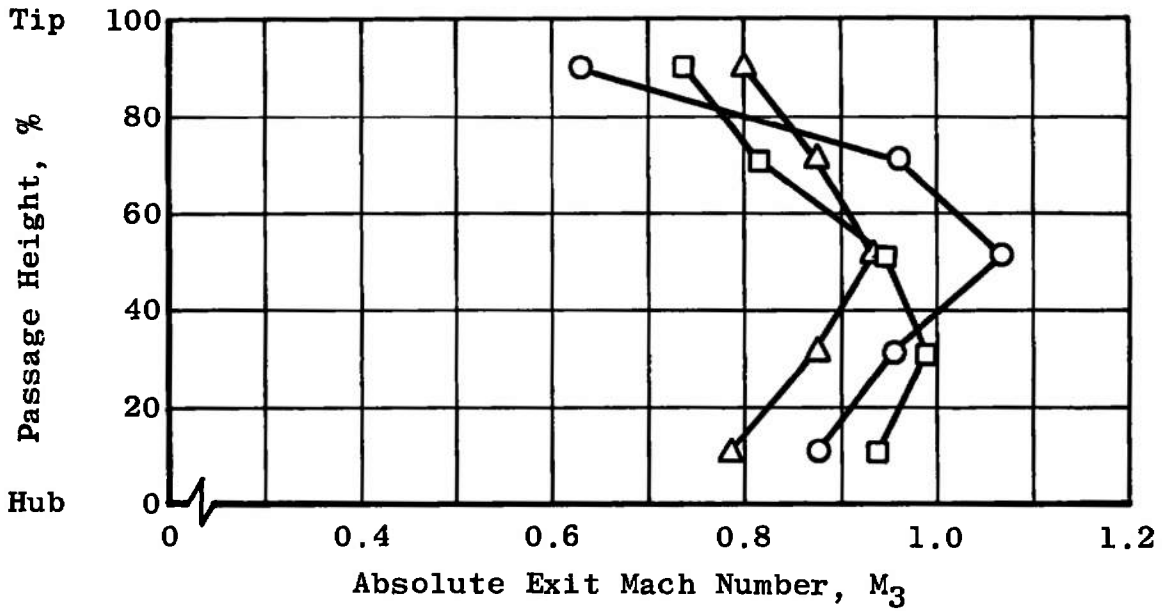

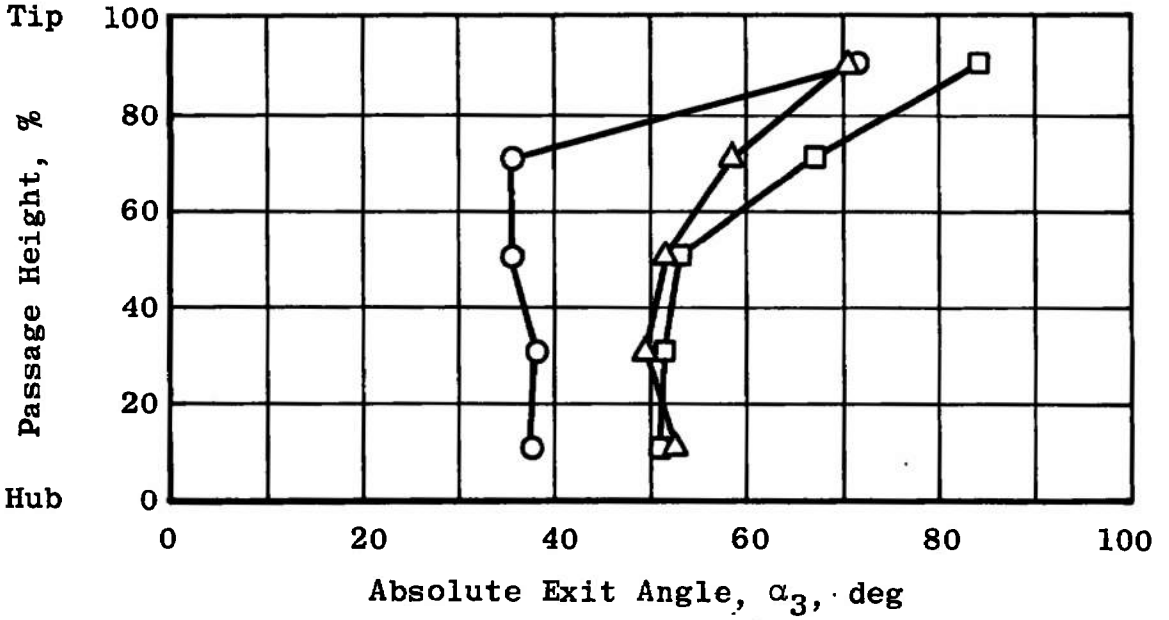

d. Exit Parameters, 100% $N/\sqrt{\theta}$

Fig. IV-1 Continued

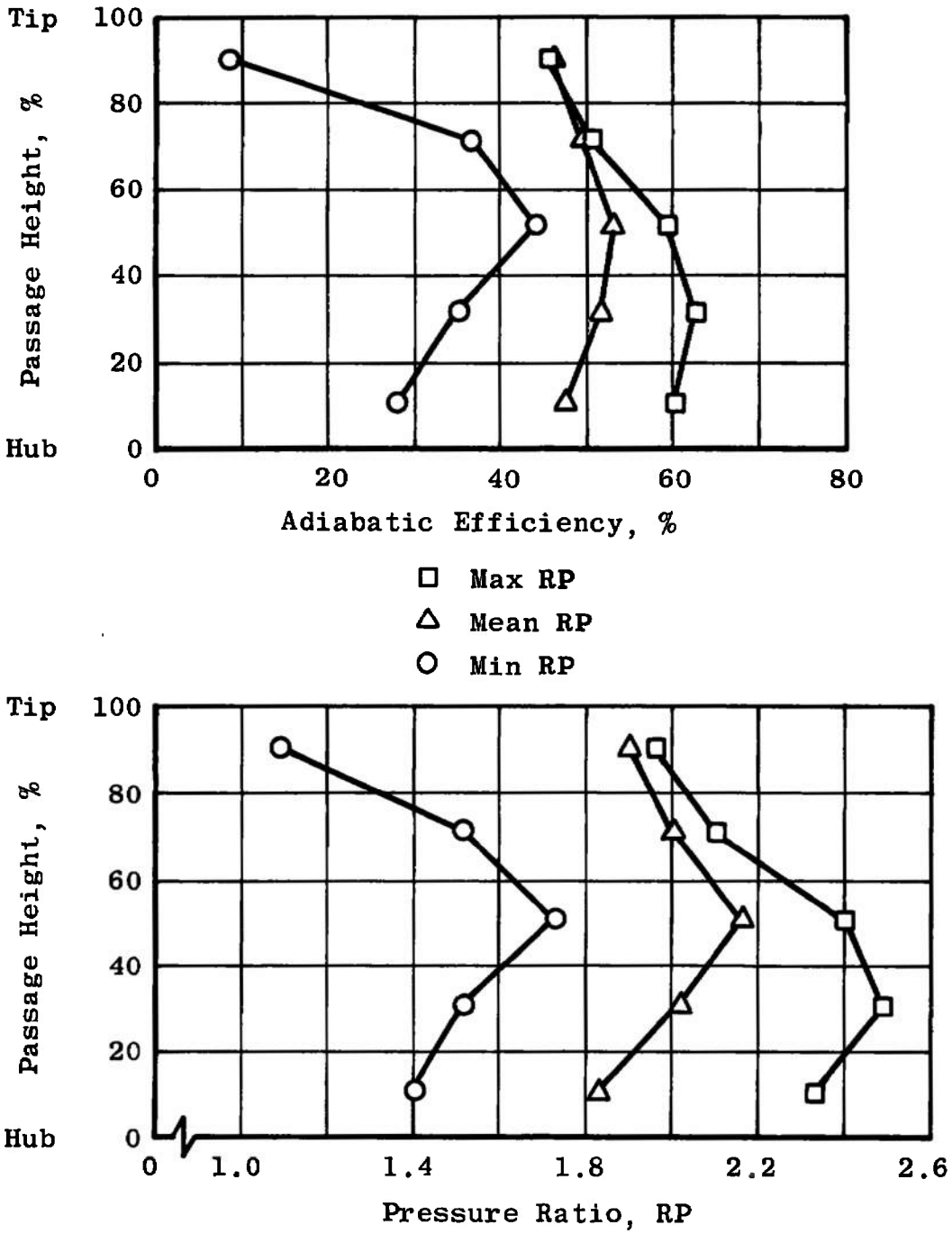

e. Adiabatic Efficiency and Pressure Ratio, 100% $N/\sqrt{\theta}$

Fig. IV-1 Continued

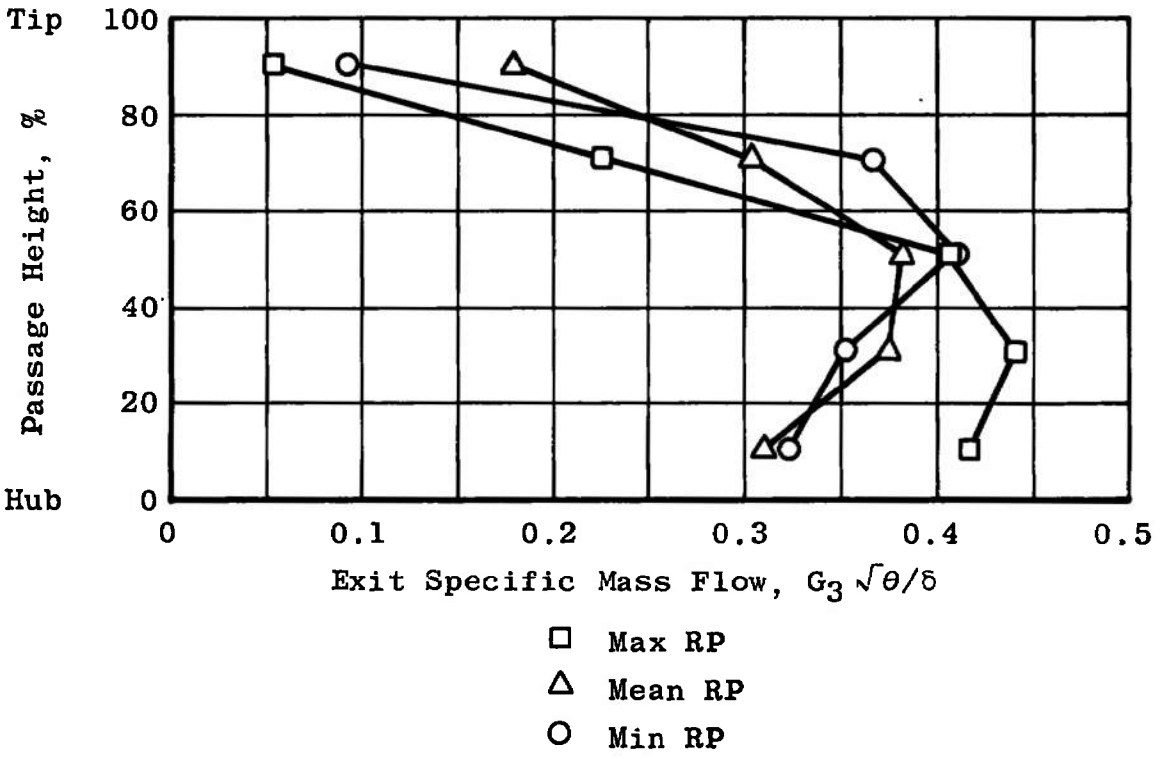

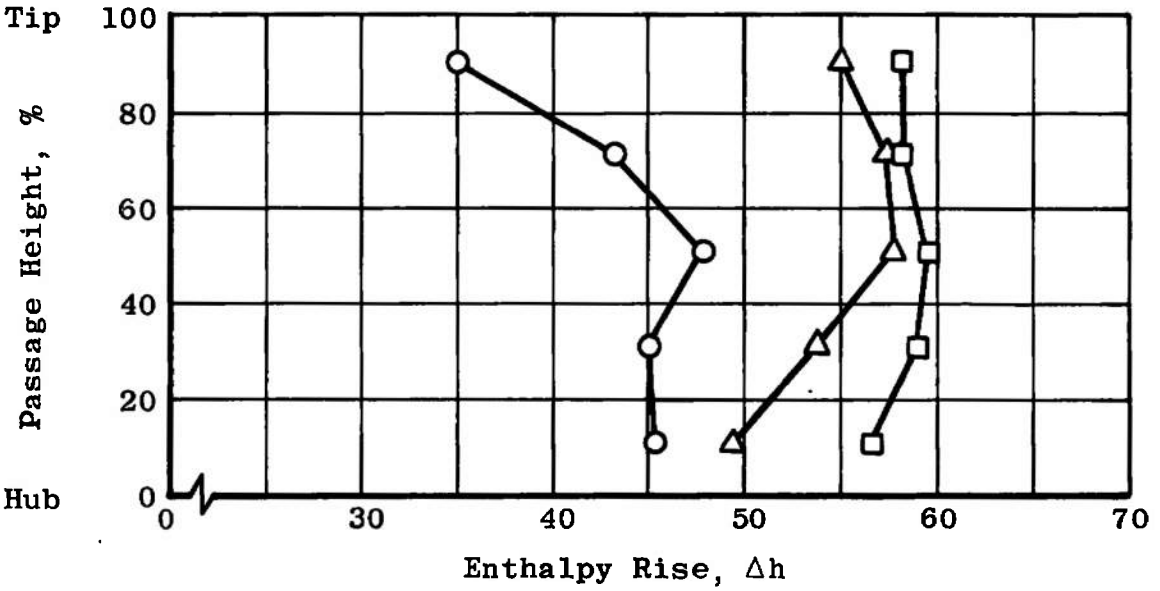

f. Exit Specific Mass Flow and Enthalpy Rise, 100% $N/\sqrt{\theta}$

Fig. IV-1 Concluded

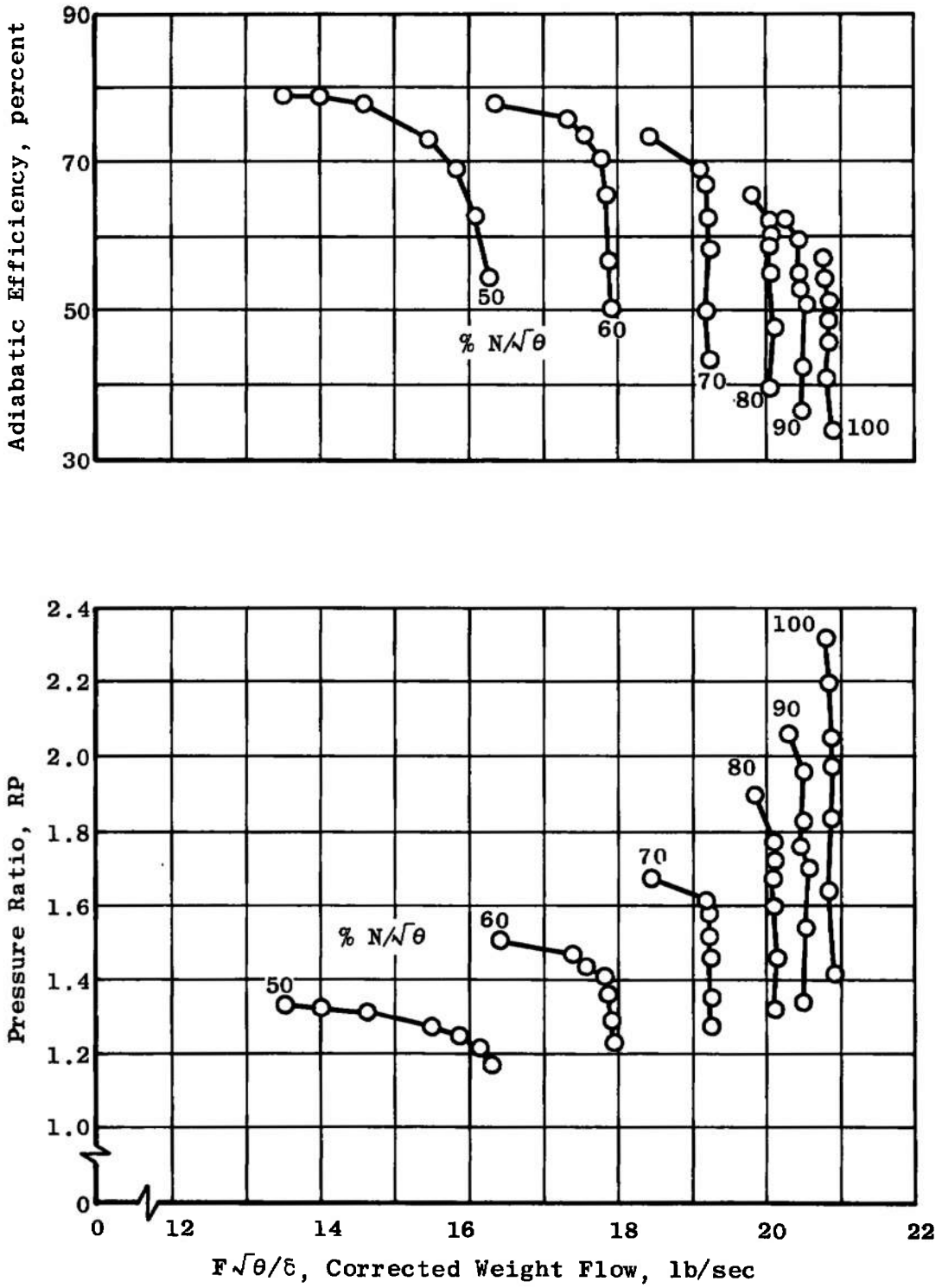

a. Compressor Performance Characteristics Based on Equivalent Weight Flow

Fig. IV-2 Configuration 2

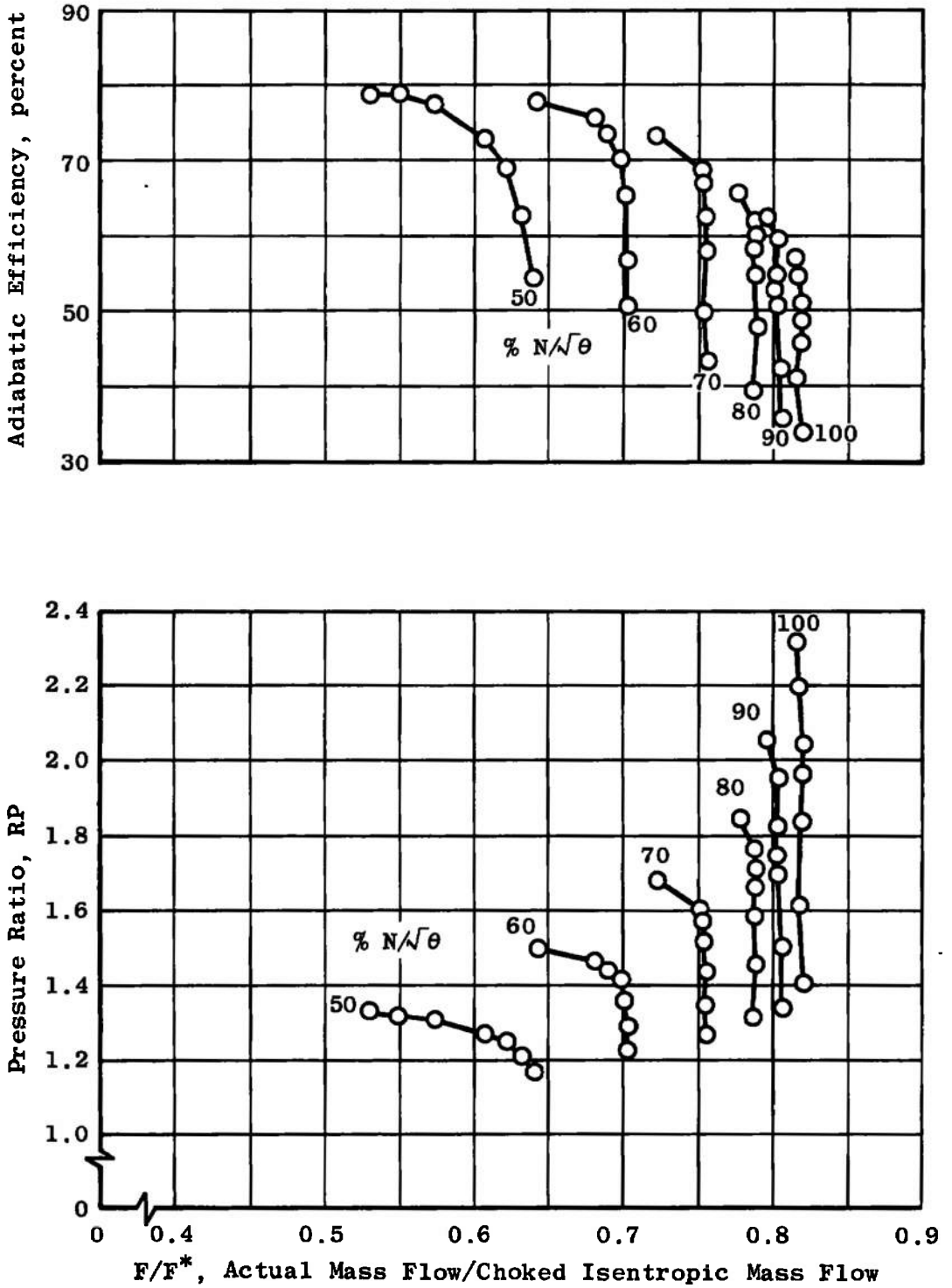

b. Compressor Performance Characteristics Based on Weight Flow Ratio

Fig. IV-2 Continued

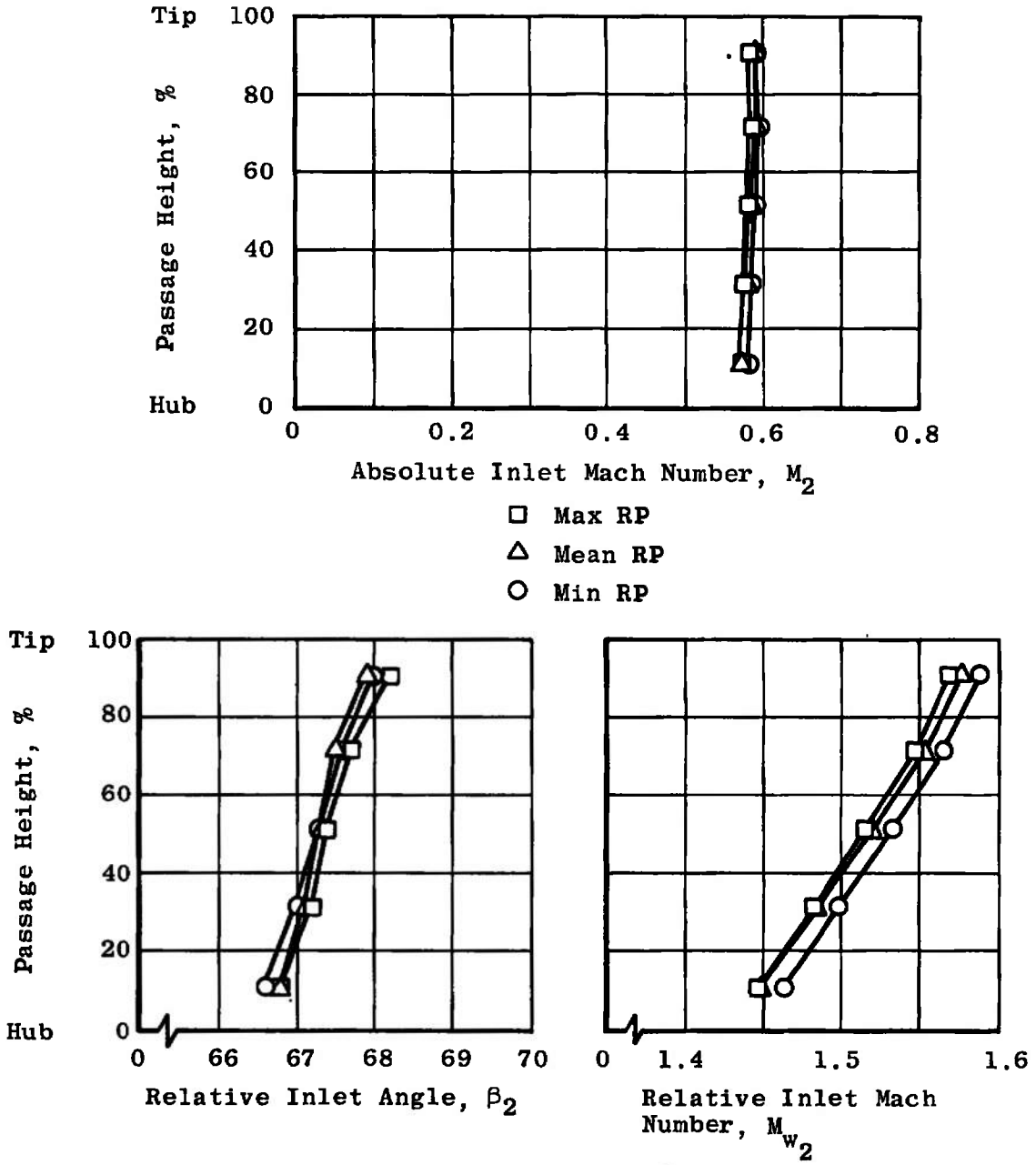

c. Inlet Parameters, 100% $N/\sqrt{\theta}$

Fig. IV-2 Continued

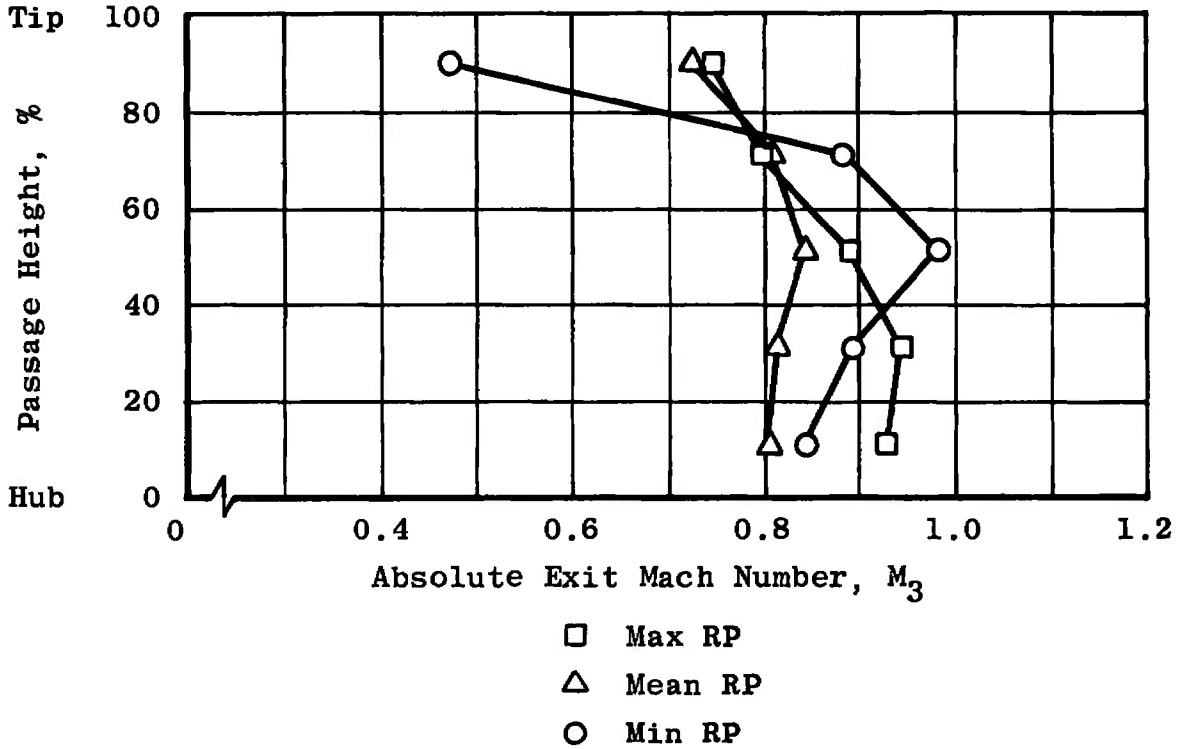

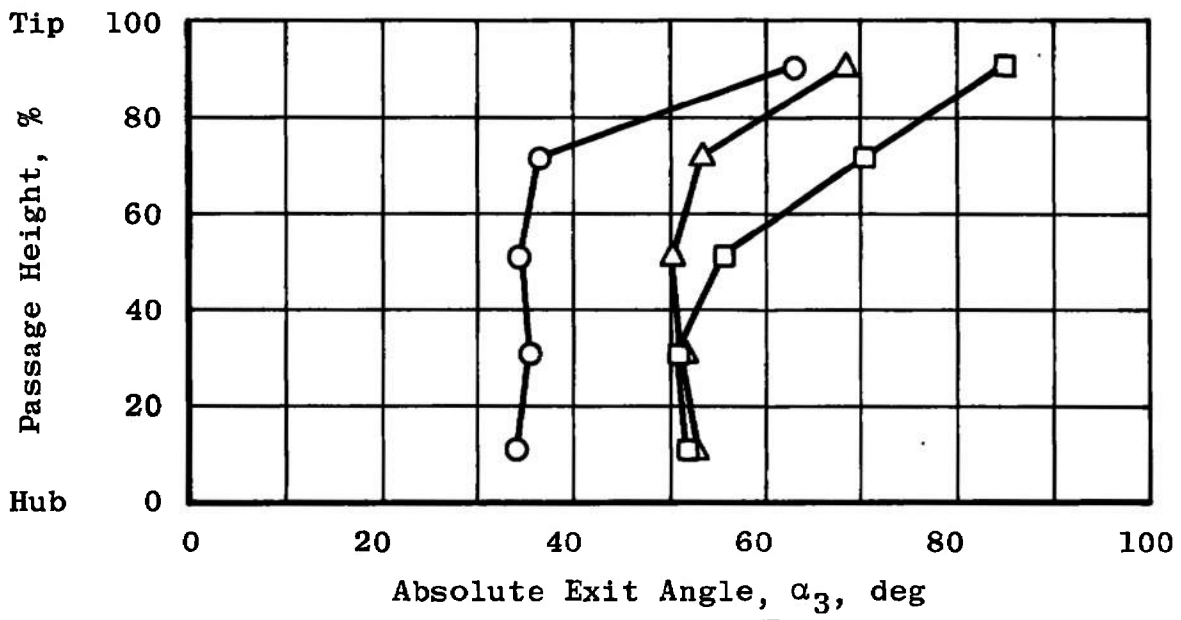

d. Exit Parameters, 100% $N/\sqrt{\theta}$

Fig. IV-2 Continued

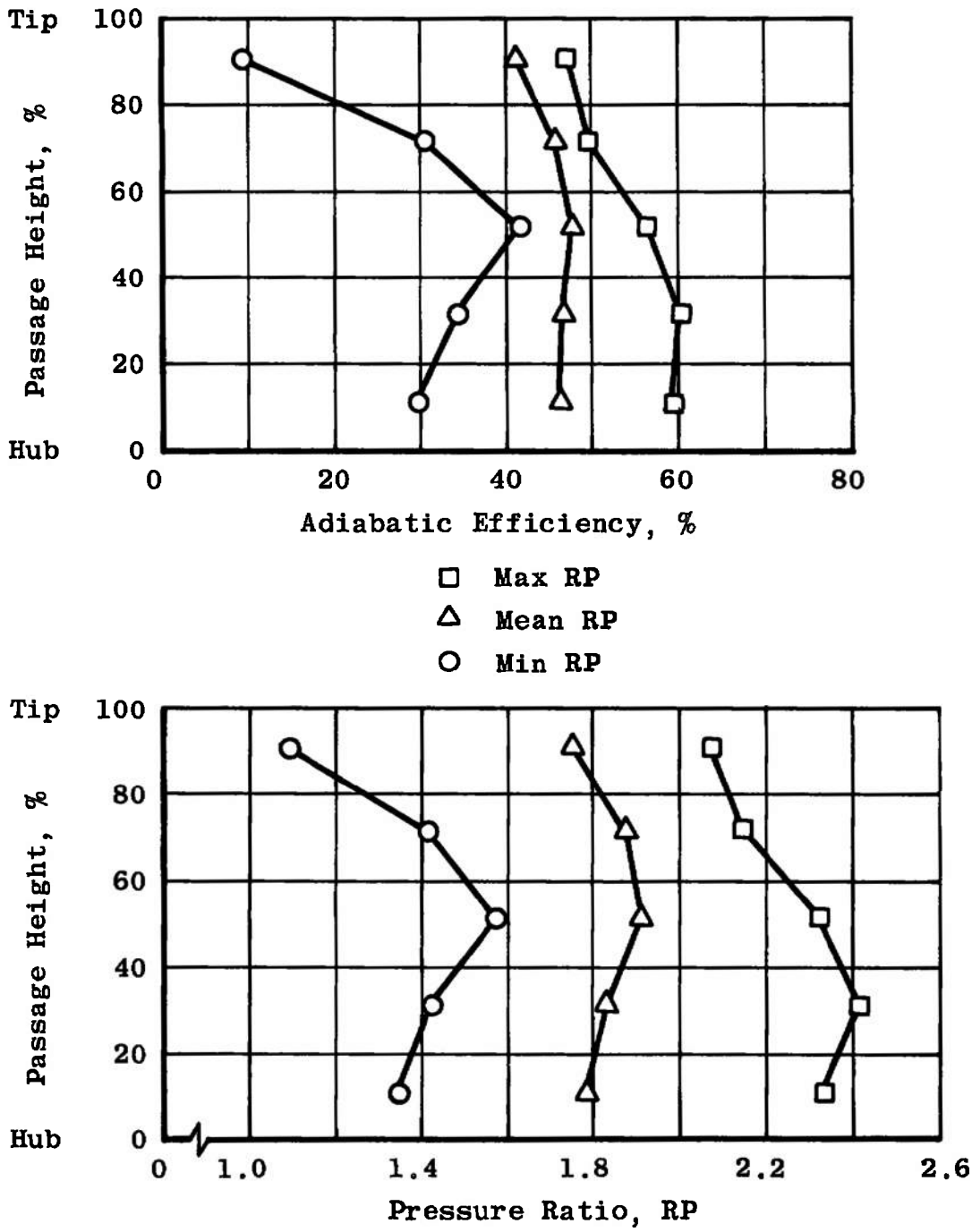

e. Adiabatic Efficiency and Pressure Ratio, 100% $N/\sqrt{\theta}$

Fig. IV-2 Continued

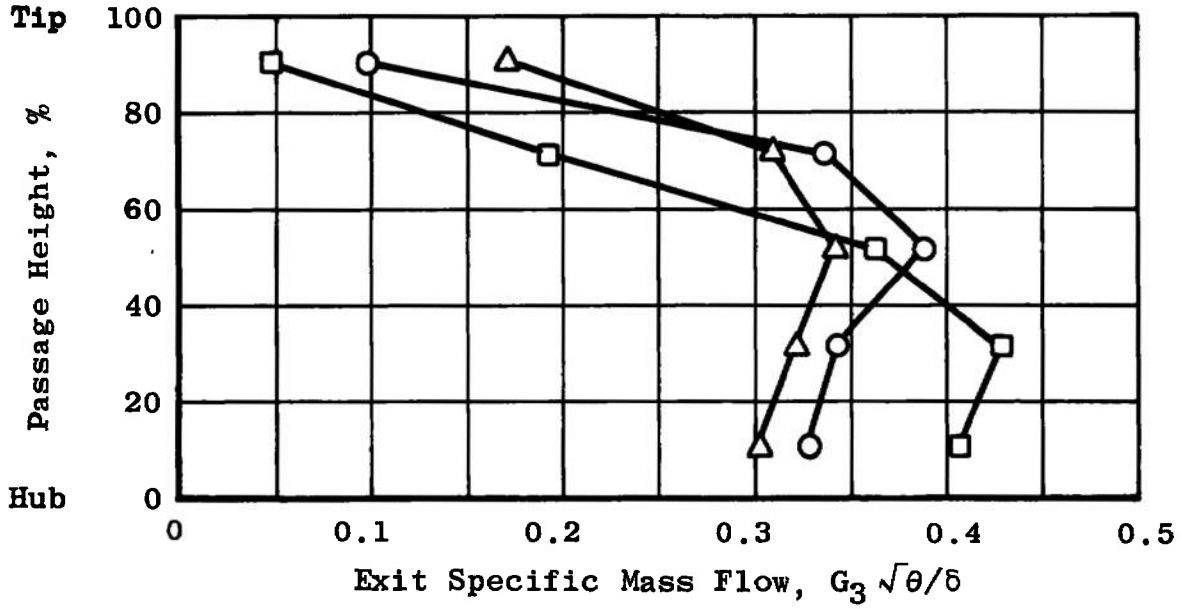

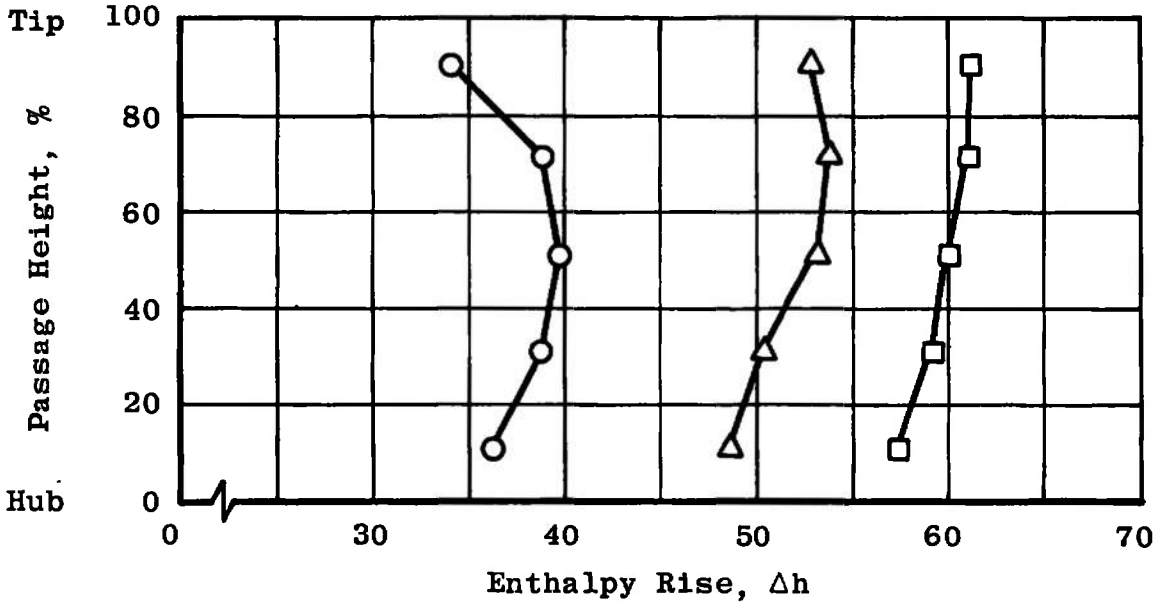

t. Exit Specific Mass Flow and Enthalpy Rise, 100% $N/\sqrt{\theta}$

Fig. IV-2 Concluded

TABLE IV-1
CONFIGURATION 1

RP	Area Centers	M_2	β_2 deg	M_{w_2}	η %	RP	M_3	α_3 deg	$G_3\frac{\sqrt{\theta}}{\delta}$	$\Delta H/\theta$
100% N										
MAXIMUM	1	0.563	68.8	1.554	45.5	1.96	0.738	84.1	0.054	58.12
	2	0.566	68.4	1.532	50.3	2.10	0.813	67.0	0.225	58.23
	3	0.561	68.1	1.505	59.2	2.40	0.948	53.1	0.406	59.58
	4	0.561	67.7	1.476	62.7	2.49	0.989	51.3	0.441	58.93
	5	0.560	67.2	1.449	60.0	2.33	0.938	51.0	0.416	56.60
MEAN	1	0.562	68.9	1.563	45.6	1.90	0.799	70.2	0.178	55.03
	2	0.563	68.6	1.540	49.2	2.05	0.877	58.2	0.303	57.44
	3	0.558	68.3	1.511	53.0	2.16	0.932	51.3	0.382	57.77
	4	0.558	67.9	1.483	51.6	2.02	0.877	49.2	0.375	53.77
	5	0.557	67.5	1.455	47.3	1.83	0.783	52.4	0.310	49.45
MINIMUM	1	0.593	67.9	1.579	8.7	1.09	0.627	71.5	0.091	34.96
	2	0.594	67.6	1.556	36.4	1.52	0.960	35.4	0.366	43.07
	3	0.594	67.2	1.528	44.1	1.73	1.069	35.5	0.409	47.81
	4	0.591	66.7	1.501	35.0	1.52	0.953	38.0	0.352	44.99
	5	0.593	66.3	1.474	27.9	1.40	0.877	37.5	0.323	45.35
90% N										
MAXIMUM	1	0.548	67.3	1.421	58.0	2.09	0.772	69.9	0.199	50.18
	2	0.554	66.7	1.404	59.2	2.11	0.791	64.5	0.253	49.89
	3	0.557	66 2	1.382	63.0	2.15	0.818	57.9	0.323	48.10
	4	0.562	65.6	1.360	65.7	2.13	0.820	54.0	0.357	45.66
	5	0.567	64.9	1.339	62.0	1.99	0.760	55.2	0.318	43.49
MEAN	1	0.580	66.3	1.441	51.9	1.81	0.703	68.3	0.180	44.14
	2	0.582	65.8	1.421	56.1	1.94	0.792	58.0	0.291	46.69
	3	0.581	65.4	1.397	60.6	2.09	0.864	54.3	0.350	48.00
	4	0.581	65.0	1.372	58.6	1.97	0.814	52.0	0.345	45.28
	5	0.580	64.5	1.348	56.2	1.84	0.752	52.5	0.313	42.01
MINIMUM	1	0.581	66.2	1.440	11.4	1.09	0.568	54.5	0.160	26.40
	2	0.578	65.9	1.416	44.4	1.51	0.920	31.2	0.391	35.07
	3	0.576	65.6	1.392	41.8	1.48	0.901	36.0	0.361	35.48
	4	0.572	65.2	1.365	34.7	1.38	0.826	36.3	0.328	34.08
	5	0.570	64.8	1.340	29.2	1.33	0.790	37.4	0.307	36.03

TABLE IV-1 (Continued)

RP	Area Centers	M_2	β_2 deg	M_{w_2}	η %	RP	M_3	α_3 deg	$G_3\sqrt{\frac{\theta}{\delta}}$	$\Delta H/\theta$
80% N										
MAXIMUM	1	0.508	66.4	1.267	64.0	1.96	0.736	66.7	0.206	41.09
	2	0.517	65.6	1.253	64.9	1.96	0.743	62.9	0.301	40.57
	3	0.523	65.0	1.235	71.2	1.97	0.758	58.3	0.320	37.46
	4	0.528	64.3	1.217	72.6	1.93	0.739	55.2	0.360	35.25
	5	0.534	63.5	1.199	68.0	1.80	0.670	60.1	0.217	33.38
MEAN	1	0.562	64.3	1.297	43.3	1.47	0.633	62.1	0.182	33.49
	2	0.562	63.9	1.278	50.4	1.61	0.745	48.1	0.306	36.20
	3	0.560	63.5	1.257	56.8	1.67	0.785	47.4	0.329	33.07
	4	0.558	63.1	1.234	53.9	1.55	0.716	44.5	0.315	30.98
	5	0.558	62.6	1.213	52.0	1.47	0.661	44.2	0.291	27.95
MINIMUM	1	0.558	64.5	1.299	38.0	1.34	0.695	43.2	0.276	28.89
	2	0.558	64.1	1.280	37.6	1.36	0.706	40.0	0.294	30.01
	3	0.558	63.7	1.259	39.0	1.35	0.705	38.0	0.302	28.72
	4	0.557	63.2	1.237	38.6	1.32	0.680	34.3	0.307	26.68
	5	0.554	62.8	1.214	27.8	1.21	0.572	43.2	0.226	24.89
70% N										
MAXIMUM	1	0.428	67.0	1.096	69.0	1.73	0.649	63.8	0.207	30.60
	2	0.438	66.2	1.084	70.7	1.74	0.662	60.2	0.237	30.18
	3	0.444	65.5	1.069	76.4	1.74	0.670	56.5	0.267	28.00
	4	0.452	64.6	1.055	77.3	1.70	0.647	54.0	0.274	26.36
	5	0.460	63.8	1.041	72.1	1.60	0.580	59.3	0.224	24.88
MEAN	1	0.517	63.1	1.143	61.0	1.51	0.598	52.5	0.241	24.96
	2	0.517	62.7	1.127	65.2	1.60	0.674	49.0	0.293	26.87
	3	0.516	62.3	1.108	66.9	1.59	0.671	48.7	0.294	24.91
	4	0.514	61.8	1.089	69.2	1.54	0.639	44.5	0.301	23.51
	5	0.512	61.4	1.070	63.2	1.42	0.547	50.5	0.228	21.99
MINIMUM	1	0.513	63.2	1.137	47.4	1.36	0.659	45.6	0.265	24.06
	2	0.514	62.7	1.121	47.2	1.37	0.670	41.3	0.288	24.68
	3	0.512	62.3	1.103	48.5	1.36	0.662	42.2	0.281	23.25
	4	0.512	61.8	1.083	49.9	1.31	0.628	36.7	0.290	20.10
	5	0.511	61.3	1.064	37.0	1.20	0.513	40.0	0.224	17.95

TABLE IV-1 (Continued)

RP	Area Centers	M_2	β_2 deg	M_{w2}	η %	RP	M_3	α_3 deg	$G_3 \frac{\sqrt{\theta}}{\delta}$	$\Delta H/\theta$
60% N										
MAXIMUM	1	0.361	67.2	0.932	71.2	1.51	0.573	61.5	0.190	21.74
	2	0.366	66.6	0.920	73.2	1.52	0.588	58.2	0.236	21.62
	3	0.370	65.9	0.907	78.5	1.52	0.593	55.7	0.236	20.16
	4	0.372	65.3	0.892	76.4	1.49	0.569	53.6	0.252	19.57
	5	0.375	64.7	0.877	72.0	1.43	0.519	57.0	0.185	18.57
MEAN	1	0.411	64.5	0.956	67.1	1.37	0.529	48.7	0.226	17.48
	2	0.416	63.9	0.944	70.6	1.43	0.591	47.2	0.259	18.95
	3	0.413	63.6	0.927	73.0	1.41	0.581	46.2	0.260	17.72
	4	0.417	62.8	0.914	72.9	1.38	0.551	41.9	0.264	16.34
	5	0.418	62.3	0.898	62.1	1.30	0.467	50.2	0.191	15.42
MINIMUM	1	0.455	62.3	0.979	44.8	1.22	0.556	36.5	0.255	16.55
	2	0.456	61.8	0.965	45.0	1.23	0.569	37.0	0.258	17.13
	3	0.454	61.4	0.949	47.4	1.24	0.574	39.4	0.252	16.37
	4	0.456	60.8	0.934	46.8	1.19	0.526	34.6	0.247	13.67
	5	0.456	60.2	0.918	38.3	1.14	0.460	37.6	0.207	12.19
50% N										
MAXIMUM	1	0.296	67.5	0.772	70.0	1.32	0.476	64.0	0.140	14.58
	2	0.304	66.5	0.764	73.6	1.34	0.504	57.0	0.209	14.74
	3	0.308	65.8	0.753	79.1	1.34	0.507	53.7	0.201	13.72
	4	0.310	65.2	0.740	78.0	1.31	0.480	50.5	0.222	12.94
	5	0.317	64.3	0.730	72.5	1.27	0.428	53.8	0.154	12.17
MEAN	1	0.350	63.8	0.801	70.2	1.26	0.475	43.4	0.216	12.11
	2	0.357	63.1	0.791	75.2	1.29	0.506	44.0	0.228	12.30
	3	0.361	62.5	0.780	73.6	1.27	0.492	45.7	0.215	12.03
	4	0.359	62.0	0.766	72.6	1.25	0.460	38.1	0.226	11.07
	5	0.357	61.6	0.752	65.0	1.20	0.394	47.4	0.168	10.21
MINIMUM	1	0.396	61.2	0.822	54.8	1.17	0.474	36.8	0.221	10.21
	2	0.397	60.7	0.811	54.6	1.18	0.494	36.9	0.229	11.00
	3	0.396	60.3	0.798	56.8	1.18	0.494	37.0	0.229	10.46
	4	0.396	59.7	0.785	57.1	1.15	0.464	32.0	0.229	9.03
	5	0.396	59.2	0.772	39.8	1.10	0.377	33.8	0.181	8.24

TABLE IV-1 (Continued)

Axial Distance, d		-2.0	-1.0	-0.25	0	0.1	0.3	0.5	0.7	0.9	1.1	1.35	1.6	2.1	2.6	3.1	4.1
100% N							RATIO OF WALL STATIC PRESSURE TO INLET TOTAL PRESSURE										
Maximum RP	O W	0.846	0.832	0.806	0.690	0.627	0.758	0.826	0.968	1.082	1.181	1.246	1.240	1.242	1.296	1.377	1.438
	I W	0.840		0.809									1.164	1.263		1.317	
Mean RP	O W	0.846	0.833	0.806	0.681	0.597	0.566	0.602	0.706	0.796	0.919	1.042	1.088	1.138	1.220	1.255	1.287
	I W	0.842		0.811									0.988	1.114		1.216	
Minimum RP	O W	0.828	0.813	0.788	0.658	0.587	0.556	0.524	0.502	0.535	0.620	0.676	0.704	0.734	0.811	0.834	0.947
	I W	0.823	0.813	0.788									0.589	0.824	0.819	0.853	0.914
90% N																	
Maximum RP	O W	0.839	0.832	0.817	0.805	0.842	0.912	1.065	1.153	1.213	1.265	1.279	1.293	1.324	1.446	1.417	1.431
	I W	0.836	0.825	0.803									1.210	1.294	1.321	1.351	1.361
Mean RP	O W	0.828	0.820	0.795	0.698	0.651	0.731	0.777	0.812	0.976	1.066	1.160	1.180	1.212	1.332	1.306	1.325
	I W	0.828	0.819	0.796									1.096	1.209	1.223	1.260	1.270
Minimum RP	O W	0.834	0.825	0.796	0.699	0.641	0.649	0.554	0.547	0.539	0.601	0.714	0.731	0.749	0.797	0.872	0.947
	I W	0.829	0.819	0.802									0.632	0.814	0.835	0.882	0.914
80% N																	
Maximum RP	O W	0.858	0.852	0.841	0.852	0.869	0.949	1.079	1.158	1.209	1.248	1.285	1.312	1.346	1.373	1.373	1.398
	I W	0.855	0.843	0.821									1.212	1.280		1.326	
Mean RP	O W	0.841	0.832	0.808	0.723	0.700	0.695	0.637	0.677	0.771	0.829	0.950	0.987	1.065	1.113	1.127	1.139
	I W	0.836	0.827	0.808									0.930	1.051	1.068	1.096	1.099
Minimum RP	O W	0.845	0.837	0.810	0.751	0.704	0.701	0.629	0.591	0.586	0.653	0.766	0.824	0.928	0.966	0.975	0.980
	I W	0.839	0.828	0.810									0.763	0.895	0.939	0.967	0.964

I W Inside Wall
O W Outside Wall

TABLE IV-1 (Concluded)

Axial Distance, d		-2.0	-1.0	-0.25	0	0.1	0.3	0.5	0.7	0.9	1.1	1.35	1.6	2.1	2.6	3.1	4.1
70% N					RATIO OF WALL STATIC PRESSURE TO INLET TOTAL PRESSURE												
Maximum	0 W	0.889	0.888	0.885	0.897	0.906	1.002	1.099	1.156	1.185	1.210	1.247	1.272	1.287	1.352	1.309	1.304
RP	1 W	0.891	0.885	0.863									1.194	1.239	1.270	1.272	1.270
Mean	0 W	0.862	0.855	0.833	0.784	0.810	0.855	0.878	0.930	0.993	1.021	1.073	1.106	1.158	1.179	1.186	1.189
RP	1 W	0.860	0.853	0.836									1.054	1.128	1.141	1.160	1.160
Minimum	0 W	0.865	0.856	0.834	0.789	0.761	0.706	0.635	0.601	0.659	0.752	0.842	0.904			1.018	
RP	1 W	0.859	0.850	0.837									0.872	0.966		1.001	
60% N																	
Maximum	0 W	0.918	0.915	0.915	0.921	0.924	0.998	1.073	1.106	1.122	1.141	1.174	1.193	1.210	1.219	1.210	1.231
RP	1 W	0.918	0.914	0.906									1.144			1.188	
Mean	0 W	0.903	0.898	0.891	0.883	0.906	0.929	0.949	0.964	0.986	1.008	1.046	1.063	1.109	1.123	1.136	1.126
RP	1 W	0.902	0.898	0.886									1.018	1.079		1.114	
Minimum	0 W	0.887	0.880	0.868	0.827	0.806	0.646	0.644	0.740	0.790	0.814	0.888	0.915			0.995	
RP	1 W	0.883	0.876	0.867									0.903	0.956		0.983	
50% N																	
Maximum	0 W	0.942	0.940	0.942	0.952	0.952	0.984	1.038	1.062	1.072	1.086	1.103	1.114	1.126	1.132	1.130	1.153
RP	1 W	0.942	0.940	0.931									1.085	1.111	1.121	1.120	1.125
Mean	0 W	0.923	0.916	0.914	0.916	0.923	0.948	0.971	0.982	0.986	0.993	1.028	1.052			1.081	
RP	1 W	0.920	0.915										1.019			1.075	
Minimum	0 W	0.909	0.904	0.897	0.879	0.862	0.855	0.861	0.870	0.872	0.876	0.933	0.944			1.002	
RP	1 W	0.910	0.905	0.898									0.936	0.976		0.992	

TABLE IV-2
CONFIGURATION 2

RP	Area Centers	M_2	β_2 deg	M_{w2}	η%	RP	M_3	α_3 deg	$G_3\frac{\sqrt{\theta}}{\delta}$	$\Delta H/\theta$
100% N										
MAXIMUM	1	0.583	68.2	1.569	47.0	2.07	0.748	85.0	0.048	61.21
	2	0.587	67.7	1.548	49.5	2.14	0.800	70.5	0.194	61.06
	3	0.581	67.4	1.515	56.2	2.32	0.891	55.8	0.364	60.00
	4	0.575	67.2	1.482	60.1	2.41	0.944	51.0	0.429	59.16
	5	0.571	66.8	1.447	59.2	2.33	0.929	52.0	0.407	57.40
MEAN	1	0.594	67.9	1.577	40.9	1.75	0.726	68.6	0.171	52.89
	2	0.594	67.5	1.554	45.4	1.87	0.809	53.5	0.309	53.82
	3	0.586	67.3	1.520	47.6	1.91	0.843	50.5	0.342	53.14
	4	0.578	67.1	1.485	46.4	1.83	0.814	51.2	0.322	50.38
	5	0.571	66.8	1.448	46.1	1.78	0.805	53.0	0.302	48.56
MINIMUM	1	0.594	68.0	1.588	9.2	1.09	0.471	63.0	0.098	34.11
	2	0.598	67.6	1.566	30.4	1.41	0.882	36.4	0.337	38.93
	3	0.592	67.3	1.533	41.5	1.57	0.981	34.2	0.389	39.83
	4	0.586	67.0	1.499	34.1	1.42	0.892	35.4	0.343	38.83
	5	0.581	66.6	1.463	29.7	1.34	0.842	34.0	0.328	36.16
90% N										
MAXIMUM	1	0.563	66.9	1.432	52.6	1.93	0.706	71.8	0.161	48.78
	2	0.568	66.3	1.411	56.1	1.97	0.746	64.5	0.233	47.49
	3	0.562	66.0	1.383	63.7	2.10	0.824	57.4	0.323	46.14
	4	0.558	65.7	1.354	66.7	2.15	0.859	53.6	0.368	45.52
	5	0.553	65.3	1.324	65.3	2.06	0.833	54.0	0.349	43.66
MEAN	1	0.576	66.4	1.440	42.9	1.59	0.686	66.7	0.170	41.30
	2	0.580	65.8	1.418	49.5	1.73	0.784	52.7	0.297	42.41
	3	0.573	65.6	1.388	54.1	1.78	0.827	48.0	0.345	41.14
	4	0.568	65.3	1.359	52.3	1.69	0.791	46.8	0.334	38.65
	5	0.561	65.0	1.327	50.1	1.63	0.763	50.3	0.297	37.14
MINIMUM	1	0.575	66.4	1.440	25.7	1.24	0.620	52.6	0.199	30.43
	2	0.581	65.8	1.419	40.3	1.41	0.774	36.7	0.330	31.84
	3	0.577	65.5	1.391	37.5	1.36	0.741	37.0	0.313	30.20
	4	0.572	65.1	1.362	38.5	1.35	0.741	36.0	0.316	28.66
	5	0.567	64.9	1.331	36.8	1.32	0.730	39.9	0.293	28.14

TABLE IV-2 (Continued)

RP	Area Centers	M_2	β_2 deg	M_{w_2}	η %	RP	M_3	α_3 deg	$G_3 \frac{\sqrt{\theta}}{\delta}$	$\Delta H/\theta$
80% N										
MAXIMUM	1	0.555	64.7	1.297	57.5	1.77	0.646	66.7	0.184	38.13
	2	0.559	64.1	1.280	62.1	1.83	0.702	61.5	0.241	37.81
	3	0.555	63.8	1.255	68.0	1.91	0.762	55.4	0.310	37.22
	4	0.549	63.4	1.228	69.5	1.89	0.762	51.8	0.335	35.67
	5	0.544	63.1	1.201	67.2	1.81	0.730	53.5	0.305	34.21
MEAN	1	0.564	64.3	1.301	48.7	1.54	0.638	64.4	0.177	33.35
	2	0.567	63.8	1.283	54.5	1.63	0.716	51.0	0.288	34.02
	3	0.563	63.4	1.258	57.6	1.64	0.737	48.0	0.314	32.83
	4	0.570	63.1	1.231	56.9	1.58	0.711	45.7	0.313	30.73
	5	0.552	62.7	1.204	54.3	1.54	0.694	49.2	0.283	30.18
MINIMUM	1	0.561	64.4	1.300	32.4	1.26	0.598	51.6	0.205	26.55
	2	0.567	63.8	1.284	40.2	1.36	0.691	40.0	0.293	28.06
	3	0.564	63.4	1.259	40.6	1.34	0.686	39.5	0.292	26.60
	4	0.559	63.0	1.233	42.7	1.32	0.683	37.0	0.300	24.28
	5	0.555	62.6	1.206	39.8	1.29	0.666	39.6	0.280	23.84
70% N										
MAXIMUM	1	0.469	65.2	1.118	64.1	1.64	0.605	65.3	0.179	29.59
	2	0.489	63.9	1.112	70.0	1.69	0.654	58.7	0.240	28.87
	3	0.492	63.3	1.093	76.6	1.73	0.691	53.2	0.293	27.58
	4	0.493	62.7	1.074	79.5	1.72	0.691	50.4	0.310	26.05
	5	0.495	62.0	1.056	72.4	1.60	0.623	54.5	0.251	24.72
MEAN	1	0.512	63.4	1.144	52.2	1.44	0.593	59.3	0.192	26.36
	2	0.527	62.3	1.135	58.3	1.50	0.650	50.6	0.261	26.12
	3	0.525	61.9	1.114	61.9	1.50	0.658	45.3	0.293	24.51
	4	0.522	61.5	1.092	61.8	1.46	0.643	43.0	0.296	23.11
	5	0.519	61.0	1.070	53.6	1.37	0.576	47.6	0.241	22.08
MINIMUM	1	0.511	63.4	1.141	37.2	1.24	0.570	47.2	0.218	21.15
	2	0.526	62.3	1.132	44.2	1.31	0.644	41.0	0.273	22.28
	3	0.525	61.8	1.112	46.2	1.31	0.655	40.0	0.281	21.48
	4	0.524	61.3	1.091	47.3	1.28	0.637	36.0	0.289	19.25
	5	0.521	60.8	1.070	39.4	1.22	0.584	39.0	0.251	18.31

TABLE IV-2 (Continued)

RP	Area Centers	M_2	β_2 deg	M_{w2}	η %	RP	M_3	α_3 deg	$G_3\frac{\sqrt{\theta}}{\delta}$	$\Delta H/\theta$
60% N										
MAXIMUM	1	0.397	65.4	0.952	68.4	1.48	0.535	63.0	0.166	21.40
	2	0.412	64.2	0.945	74.7	1.52	0.582	55.8	0.224	21.08
	3	0.415	63.5	0.929	81.6	1.54	0.606	51.0	0.261	19.87
	4	0.418	62.8	0.914	83.0	1.51	0.595	48.5	0.268	18.75
	5	0.422	62.0	0.898	78.7	1.46	0.559	54.0	0.222	18.04
MEAN	1	0.463	62.0	0.985	55.8	1.33	0.523	56.0	0.184	19.00
	2	0.470	61.2	0.975	64.7	1.38	0.582	45.3	0.257	18.59
	3	0.466	60.8	0.955	68.9	1.39	0.593	42.0	0.277	17.61
	4	0.464	60.3	0.938	69.8	1.37	0.587	40.5	0.279	16.83
	5	0.462	59.9	0.919	64.7	1.33	0.550	47.0	0.233	16.13
MINIMUM	1	0.461	62.1	0.985	41.2	1.20	0.503	48.6	0.192	15.92
	2	0.472	61.1	0.977	50.8	1.25	0.574	39.8	0.255	16.33
	3	0.470	60.7	0.959	53.1	1.25	0.580	37.5	0.266	15.61
	4	0.468	60.2	0.941	52.9	1.24	0.571	34.6	0.270	14.83
	5	0.466	59.7	0.923	50.4	1.21	0.550	40.5	0.240	14.04
50% N										
MAXIMUM	1	0.317	66.4	0.790	70.0	1.32	0.460	63.3	0.135	14.64
	2	0.329	65.1	0.782	76.5	1.34	0.497	55.5	0.184	14.34
	3	0.335	64.3	0.771	82.7	1.35	0.514	51.3	0.210	13.54
	4	0.339	63.5	0.758	82.9	1.33	0.499	48.6	0.215	12.80
	5	0.342	62.7	0.745	78.2	1.30	0.465	51.4	0.188	12.25
MEAN	1	0.403	61.0	0.831	62.2	1.23	0.457	48.0	0.189	12.36
	2	0.412	60.0	0.824	68.9	1.26	0.501	42.6	0.228	12.48
	3	0.412	59.4	0.810	72.3	1.27	0.511	40.2	0.241	12.02
	4	0.410	59.0	0.795	72.7	1.25	0.500	38.6	0.240	11.34
	5	0.408	58.5	0.780	68.0	1.22	0.464	46.0	0.197	10.56
MINIMUM	1	0.417	60.2	0.838	44.9	1.15	0.445	45.4	0.182	11.23
	2	0.424	59.3	0.830	54.5	1.19	0.500	36.2	0.235	11.38
	3	0.423	58.8	0.815	58.5	1.19	0.512	35.6	0.242	10.88
	4	0.421	58.3	0.801	59.7	1.18	0.509	34.6	0.243	10.29
	5	0.417	57.9	0.784	51.1	1.15	0.464	40.5	0.204	9.59

TABLE IV-2 (Continued)

Axial Distance, d		-2.0	-1.0	-0.25	0	0.1	0.3	0.5	0.7	0.9	1.1	1.35	1.6	2:1	2.6	3.1	4.1
100% N		RATIO OF WALL STATIC PRESSURE TO INLET TOTAL PRESSURE															
Maximum	0 W	0.828	0.814	0.789	0.699	0.712	0.872	1.076	1.101	1.270	1.298	1.274	1.275	1.301	1.361	1.445	1.489
RP	1 W	0.825	0.818	0.804								1.143	1.238	1.270	1.273	1.325	1.361
Mean	0 W	0.824	0.811	0.784	0.684	0.544	0.514	0.554	0.687	0.884	0.978	1.002	1.049	1.116	1.198	1.246	1 257
RP	1 W	0.823	0.816	0.803								0.890	0.987	1.122	1.130	1.157	1.177
Minimum	0 W	0.825	0.810	0.783	6.87	0.544	0.502	0.442	0.402	0.425	0.596	0.666	0.667	0.726	0.813	0.857	0.936
RP	1 W	0.824	0.814	0.796								0.548	0.606	0.806	0.806	0.841	0.904
90% N																	
Maximum	0 W	0.829	0.823	0.801	0.743	0.764	0.872	1.063	1.086	1.167	1.261	1.277	1.280	1.289	1.361	1.395	1.412
RP	1 W	0.841	0.831	0.815								1.169	1.221	1.269	1.266	1.299	1.316
Mean	0 W	0.824	0.820	0.793	0.713	0.591	0.612	0.532	0.675	0.837	0.931	1.015	1.036	1.049	1.132	1.173	1.194
RP	1 W	0.831	0.822	0.810								0.911	0.980	1.077	1.076	1.101	1.126
Minimum	0 W	0.825	0.819	0.793	0.717	0.593	0.607	0.473	0.455	0.522	0.662	0.748	0.771	0.826	0.921	0.960	0.981
RP	1 W	0.832	0.823	0.806								0.683	0.740	0.885	0.898	0.926	0.945
80% N																	
Maximum	0 W	0.840	0.829	0.807	0.751	0.766	0.857	0.896	1.019	1.083	1.177	1.246	1.252	1.270	1.320	1.343	1.345
RP	1 W	0.846	0.837	0.819								1.152	1.204	1.250	1.242	1.263	1.280
Mean	0 W	0.836	0.828	0.802	0.739	0.651	0.648	0.578	0.710	0.836	0.927	1.029	1.065	1.090	1.158	1.176	1.175
RP	1 W	0.839	0.829	0.814								0.957	1.015	1.100	1.096	1.112	1.127
Minimum	0 W	0.838	0.827	0.803	0.742	0.652	0.641	0.489	0.499	0.580	0.709	0.782	0.809	0.896	0.972	0.998	0.990
RP	1 W	0.838	0.830	0.812								0.751	0.813	0.919	0.934	0.990	0.964

TABLE IV-2 (Concluded)

Axial Distance, d		-2.0	-1.0	-0.25	0	0.1	0.3	0.5	0.7	0.9	1.1	1.35	1.6	2:1	2.6	3.1	4.1
70% N																	
Maximum RP	0 W	0.870	0.862	0.853	0.842	0.875	0.947	1.060	1.081	1.124	1.183	1.217	1.234	1.251	1.280	1.291	1.296
	1 W	0.876	0.870	0.846								1.137	1.176	1.218	1.224	1.227	1.240
Mean RP	0 W	0.859	0.849	0.828	0.785	0.721	0.669	0.644	0.723	0.854	0.957	1.027	1.077	1.111	1.132	1 144	1.142
	1 W	0.857	0.851	0.834								0.976	1.019	1.087	1.096	1.093	1.100
Minimum RP	0 W	0.859	0.849	0.829	0.784	0.720	0.657	0.517	0.536	0.686	0.761	0.819	0.868	0.948	0.983	0.998	0.996
	1 W	0.859	0.851	0.833								0.809	0.858	0.947	0.961	0.964	0.967
60% N																	
Maximum RP	0 W	0.899	0.896	0.894	0.899	0.911	0.967	1.045	1.065	1.096	1.137	1.168	1.188	1.192	1 214	1.220	1.217
	1 W	0.904	0.902	0.885								1.112	1.132	1.175	1.167	1.176	1.182
Mean RP	0 W	0.877	0.874	0.859	0.820	0.762	0.655	0.734	0.818	0.874	0.967	1.033	1.065	1.081	1.103	1.109	1.100
	1 W	0.879	0.875	0.866								0.995	1.024	1.068	1.066	1.016	1.070
Minimum RP	0 W	0.880	0.874	0.859	0.819	0.759	0.606	0.541	0.684	0.786	0.826	0.883	0.938	0.979	0.997	1.010	1.006
	1 W	0.879	0.874	0.864								0.878	0.919	0.977	0.982	0.986	0.984
50% N																	
Maximum RP	0 W	0.931	0.930	0.930	0.936	0.944	0.968	1.030	1.045	1.070	1.095	1.113	1.122	1.132	1.146	1.144	1.145
	1 W	0.936	0.935	0.922								1.078	1.085	1.113	1.118	1.115	1.120
Mean RP	0 W	0.903	0.899	0.889	0.867	0.821	0.842	0.868	0.899	0.927	0.973	1.029	1.047	1.064	1.075	1.072	1.070
	1 W	0.909	0.906	0.893								1.004	1.017	1.045	1.054	1.048	1.052
Minimum RP	0 W	0.898	0.896	0.883	0.850	0.750	0.585	0.697	0.788	0.825	0.864	0.921	0.960	0.994	1.006	1.005	1.003
	1 W	0.903	0.900	0.889								0.932	0.945	0.979	0.991	0.986	0.987

UNCLASSIFIED
Security Classification

DOCUMENT CONTROL DATA - R & D

(Security classification of title, body of abstract and indexing annotation must be entered when the overall report is classified)

1 ORIGINATING ACTIVITY *(Corporate author)*
Arnold Engineering Development Center
ARO, Inc., Contract Operator
Arnold Air Force Station, Tennessee

2a. REPORT SECURITY CLASSIFICATION
UNCLASSIFIED

2b. GROUP
N/A

3 REPORT TITLE
EXPERIMENTAL INVESTIGATION OF TWO BLUNT TRAILING EDGE SUPERSONIC COMPRESSOR ROTORS OF DIFFERENT BLADE THICKNESSES AND WITH CIRCULAR ARC CAMBER LINE

4 DESCRIPTIVE NOTES *(Type of report and inclusive dates)*

5 AUTHOR(S) *(First name, middle initial, last name)*
C. T. Carman and J. R. Myers, ARO, Inc., and A. J. Wennerstrom and John W. Steurer, Aerospace Research Laboratories

6 REPORT DATE
September 1968

7a. TOTAL NO. OF PAGES
58

7b. NO OF REFS
5

8a. CONTRACT OR GRANT NO
F40600-69-C-0001

b. PROJECT NO
7065

c. Program Element 6144501F

d

9a. ORIGINATOR'S REPORT NUMBER(S)
AEDC-TR-68-197

9b. OTHER REPORT NO(S) *(Any other numbers that may be assigned this report)*
N/A

10 DISTRIBUTION STATEMENT
This document has been approved for public release and sale; its distribution is unlimited.

11 SUPPLEMENTARY NOTES
Available in DDC.

12. SPONSORING MILITARY ACTIVITY
Arnold Engineering Development Center, Air Force Systems Command, Arnold Air Force Station, Tennessee

13 ABSTRACT

Two configurations of blunt-trailing-edge supersonic compressor blades were tested with air in the AEDC compressor rig. The performance of these blades was investigated over the speed range from 50 to 100 percent of design speed. The performance of the two blade configurations is compared, and the effect of the modifications between the two configurations is evaluated.

DD FORM 1 NOV 65 1473

UNCLASSIFIED
Security Classification

14 KEY WORDS	LINK A ROLE	LINK A WT	LINK B ROLE	LINK B WT	LINK C ROLE	LINK C WT
supersonic compressors						
compressor rotors						
compressor blades						
blunt trailing edge						
performance						
pressure distribution	1	2				
Mach number distribution						

1. Rotors -- Trailing edges
2 Blades -- " "
3 Blades -- Pressure distribution
4 " -- Mach velocity distribution